Corrections

MEDICAL SCIENCES

Correction for "NF-κB inhibits osteogenic differentiation of mesenchymal stem cells by promoting β-catenin degradation," by Jia Chang, Fei Liu, Min Lee, Benjamin Wu, Kang Ting, Janette N. Zara, Chia Soo, Khalid Al Hezaimi, Weiping Zou, Xiaohong Chen, David J. Mooney, and Cun-Yu Wang, which appeared in issue 23, June 4, 2013, of *Proc Natl Acad Sci USA* (110:9469–9474; first published May 20, 2013; 10.1073/pnas.1300532110).

The authors note that Fig. 1 appeared incorrectly. The corrected figure and its legend appear below. This error does not affect the conclusions of the article.

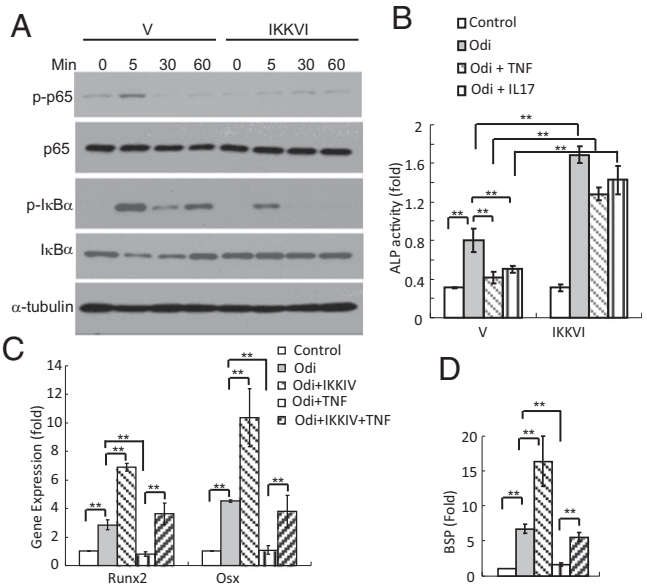

Fig. 1. The IKKβ small molecule inhibitor, IKKVI, promotes osteogenic differentiation by inhibiting NF-κB. (*A*) IKKVI inhibited IKK activities induced by TNF in mMSCs. Cells were pretreated with IKKVI or vehicle control for 30 min and then treated with TNF for the indicated times. The phosphorylation and degradation of IκBα and p65 phosphorylation were examined by Western blot. (*B*) IKKVI overcame TNF and IL-17 inhibition of ALP in mMSCs by inhibiting NF-κB. The results are the average value from three independent experiments and presented as mean ± SD. **P < 0.01. Odi, osteogenic differentiation-inducing media. (*C*) IKKVI attenuated TNF inhibition of Runx2 and Osx by inhibiting NF-κB in mMSCs, as assessed by Real-time RT-PCR. P < 0.01. (*D*) IKKVI attenuated TNF inhibition of BSP induction by inhibiting NF-κB in mMSCs.

www.pnas.org/cgi/doi/10.1073/pnas.1313266110

NEUROSCIENCE

Correction for "Aβ induces astrocytic glutamate release, extrasynaptic NMDA receptor activation, and synaptic loss," by Maria Talantova, Sara Sanz-Blasco, Xiaofei Zhang, Peng Xia, Mohd Waseem Akhtar, Shu-ichi Okamoto, Gustavo Dziewczapolski, Tomohiro Nakamura, Gang Cao, Alexander E. Pratt, Yeon-Joo Kang, Shichun Tu, Elena Molokanova, Scott R. McKercher, Samuel Andrew Hires, Hagit Sason, David G. Stouffer, Matthew W. Buczynski, James P. Solomon, Sarah Michael, Evan T. Powers, Jeffery W. Kelly, Amanda Roberts, Gary Tong, Traci Fang-Newmeyer, James Parker, Emily A. Holland, Dongxian Zhang, Nobuki Nakanishi, H.-S. Vincent Chen, Herman Wolosker, Yuqiang Wang, Loren H. Parsons, Rajesh Ambasudhan, Eliezer Masliah, Stephen F. Heinemann, Juan C. Piña-Crespo, and Stuart A. Lipton, which appeared in issue 27, July 2, 2013, of *Proc Natl Acad Sci USA* (110:E2518–E2527; first published June 17, 2013; 10.1073/pnas.1306832110).

The authors note that their conflict of interest statement was omitted during publication. The authors declare that "S.A.L. is the inventor on world-wide patents for the use of memantine and NitroMemantine for neurodegenerative disorders; Y.W. is also a named inventor on the patents for NitroMemantine. Per Harvard University guidelines, S.A.L. participates in a royalty-sharing agreement with his former institution Boston Children's Hospital/Harvard Medical School, which licensed the drug memantine (Namenda) to Forest Laboratories, Inc."

www.pnas.org/cgi/doi/10.1073/pnas.1313546110

STATISTICS

Correction for "Using distance correlation and SS-ANOVA to assess associations of familial relationships, lifestyle factors, diseases, and mortality," by Jing Kong, Barbara E. K. Klein, Ronald Klein, Kristine E. Lee, and Grace Wahba, which appeared in issue 50, December 11, 2012, of *Proc Natl Acad Sci USA* (109:20352–20357; first published November 21, 2012; 10.1073/pnas.1217269109).

The authors note that: "The phrase 'non-Euclidean pedigree dissimilarity'" on page 20355, right column, first paragraph, line 3, is not correct. As a result of the error, the text from page 20355, right column, line 1 to page 20365, right column, line 7, and Figs 3 and 4 are superfluous and should be omitted.

"The pedigree dissimilarity in the article is in fact Euclidean, a consequence of the fact that the matrix of kinship coefficients $\{\varphi_{ij}\}$ is positive definite, a fact that has been long since known. Thus, there is no reason to invoke the pedigree embedding by regularized kernel estimation (RKE), and the striking similarity between *Upper* and *Lower* of Fig. 3, and also between Figs. 2 and 4, is not surprising. In theory, they should be identical. The very minor differences can be explained by the small amount of regularization applied here in the RKE method. The rest of the paper, including results and discussion, is not affected. We thank Daniel Gianola and Gustavo de los Campos for pointing out the mistake."

www.pnas.org/cgi/doi/10.1073/pnas.1313265110

Aβ induces astrocytic glutamate release, extrasynaptic NMDA receptor activation, and synaptic loss

Maria Talantova[a,1], Sara Sanz-Blasco[a,1], Xiaofei Zhang[a,1], Peng Xia[a,1], Mohd Waseem Akhtar[a], Shu-ichi Okamoto[a], Gustavo Dziewczapolski[b], Tomohiro Nakamura[a], Gang Cao[a], Alexander E. Pratt[a,c], Yeon-Joo Kang[a], Shichun Tu[a], Elena Molokanova[a], Scott R. McKercher[a], Samuel Andrew Hires[d], Hagit Sason[e], David G. Stouffer[f], Matthew W. Buczynski[f], James P. Solomon[g,h,i], Sarah Michael[c], Evan T. Powers[g,h,i], Jeffery W. Kelly[g,h,i], Amanda Roberts[j], Gary Tong[a,2], Traci Fang-Newmeyer[a], James Parker[a], Emily A. Holland[a], Dongxian Zhang[a], Nobuki Nakanishi[a], H.-S. Vincent Chen[a], Herman Wolosker[e], Yuqiang Wang[k,l], Loren H. Parsons[f], Rajesh Ambasudhan[a], Eliezer Masliah[c], Stephen F. Heinemann[b,3], Juan C. Piña-Crespo[a,3], and Stuart A. Lipton[a,b,c,h,3]

[a]Del E. Webb Center for Neuroscience, Aging, and Stem Cell Research, Sanford-Burnham Medical Research Institute, La Jolla, CA 92037; [b]Molecular Neurobiology Laboratory, Salk Institute for Biological Studies, La Jolla, CA 92037; [c]Department of Neurosciences, School of Medicine, University of California San Diego, La Jolla, CA 92039; [d]Janelia Farm Research Campus, Howard Hughes Medical Research Institute, Ashburn, VA 20147; [e]Department of Biochemistry, Technion-Israel Institute of Technology, Haifa 31096, Israel; [f]Committee on the Neurobiology of Addictive Disorders, The Scripps Research Institute, La Jolla, CA 92037; Departments of [g]Chemistry, [h]Molecular and Experimental Medicine, and [i]Skaggs Institute for Chemical Biology, The Scripps Research Institute, La Jolla, CA 92037; [j]Department of Molecular and Cellular Neuroscience, The Scripps Research Institute, La Jolla, CA 92037; [k]Institute of New Drug Research, Jinan University College of Pharmacy, Guangzhou 510632, China; and [l]Panorama Research Inc., Sunnyvale, CA 94089

Contributed by Stephen F. Heinemann, April 16, 2013 (sent for review February 16, 2013)

Synaptic loss is the cardinal feature linking neuropathology to cognitive decline in Alzheimer's disease (AD). However, the mechanism of synaptic damage remains incompletely understood. Here, using FRET-based glutamate sensor imaging, we show that amyloid-β peptide (Aβ) engages α7 nicotinic acetylcholine receptors to induce release of astrocytic glutamate, which in turn activates extrasynaptic NMDA receptors (eNMDARs) on neurons. In hippocampal autapses, this eNMDAR activity is followed by reduction in evoked and miniature excitatory postsynaptic currents (mEPSCs). Decreased mEPSC frequency may reflect early synaptic injury because of concurrent eNMDAR-mediated NO production, tau phosphorylation, and caspase-3 activation, each of which is implicated in spine loss. In hippocampal slices, oligomeric Aβ induces eNMDAR-mediated synaptic depression. In AD-transgenic mice compared with wild type, whole-cell recordings revealed excessive tonic eNMDAR activity accompanied by eNMDAR-sensitive loss of mEPSCs. Importantly, the improved NMDAR antagonist NitroMemantine, which selectively inhibits extrasynaptic over physiological synaptic NMDAR activity, protects synapses from Aβ-induced damage both in vitro and in vivo.

α7-nicotinics | astrocytes | glutamate receptors

Emerging evidence suggests that the injurious effects of amyloid β peptide (Aβ) in Alzheimer's disease (AD) may be mediated, at least in part, by excessive activation of extrasynaptic or perisynaptic NMDARs (eNMDARs) containing predominantly NR2B subunits (1, 2). In contrast, in several neurodegenerative paradigms, physiological synaptic NMDAR (sNMDAR) activity can be neuroprotective (refs. 3–8, but see ref. 9). Soluble oligomers of $A\beta_{1–42}$ are thought to underlie dementia, mimic extracellular glutamate stimulation of eNMDARs, and disrupt synaptic plasticity and long-term potentiation, eventually leading to synaptic loss (1, 6, 10, 11). However, mechanistic insight into the action of Aβ that causes excessive eNMDAR stimulation and the potential link between eNMDARs and synaptic damage remain to be elucidated. Here, we examine the cascade involved in eNMDAR activation by oligomeric Aβ and its consequences on miniature excitatory postsynaptic currents (mEPSCs). We found that eNMDAR activation is triggered by extrasynaptic glutamate released from astrocytes in response to Aβ peptide. In turn, eNMDAR stimulation is followed rapidly by a decrease in mEPSC frequency with accompanying generation of nitric oxide (NO), hyperphosphorylation of tau, and activation of caspase-3. Pharmacological blockade of eNMDARs with relative sparing of sNMDARs abrogated NO production, tau phosphorylation, caspase activation, and subsequent synaptic loss. These results suggest a glutamate-mediated cascade triggered by Aβ in which early eNMDAR activation may contribute to subsequent synaptic damage and consequent cognitive decline in AD.

Results

FRET-Based Imaging of Aβ-Induced Glutamate Release from Cultured Astrocytes. Inflammatory cells, including microglia and astrocytes, are thought to contribute to damage in AD, in part via glutamate excitotoxicity (2, 12). For example, exposure to oligomeric Aβ or conditioned medium from microglial cultures incubated with Aβ has been reported to decrease glutamate reuptake from astrocytes in brain slices and cultures (13–16), but whether Aβ also induces local release of toxic glutamate levels onto neurons remains unknown. To study this question, we used a FRET-based

Significance

Communication between nerve cells occurs at specialized cellular structures known as synapses. Loss of synaptic function is associated with cognitive decline in Alzheimer's disease (AD). However, the mechanism of synaptic damage remains incompletely understood. Here we describe a pathway for synaptic damage whereby amyloid-$\beta_{1–42}$ peptide ($A\beta_{1–42}$) releases, via stimulation of α7 nicotinic receptors, excessive amounts of glutamate from astrocytes, in turn activating extrasynaptic NMDA-type glutamate receptors (eNMDARs) to mediate synaptic damage. The Food and Drug Administration-approved drug memantine offers some beneficial effect, but the improved eNMDAR antagonist NitroMemantine completely ameliorates Aβ-induced synaptic loss, providing hope for disease-modifying intervention in AD.

Author contributions: M.T., S.S.-B., J.C.P.-C., and S.A.L. designed research; M.T., S.S.-B., X.Z., P.X., M.W.A., S.-i.O., G.D., G.C., A.E.P., Y.-J.K., S.T., E. Molokanova, S.R.M., S.A.H., H.S., D.G.S., M.W.B., J.P.S., S.M., A.R., G.T., T.F.-N., J.P., E.A.H., H.W., Y.W., and R.A. performed research; M.T., S.S.-B., X.Z., P.X., M.W.A., S.-i.O., G.D., T.N., G.C., A.E.P., Y.-J.K., S.T., E. Molokanova, S.R.M., S.A.H., H.S., D.G.S., M.W.B., J.P.S., S.M., E.T.P., J.W.K., A.R., G.T., T.F.-N., J.P., E.A.H., D.Z., N.N., H.-S.V.C., H.W., L.H.P., R.A., E. Masliah, S.F.H., J.C.P.-C., and S.A.L. analyzed data; D.Z., N.N., H.-S.V.C., and S.F.H. interpreted data; and T.N., E.T.P., J.W.K., H.W., L.H.P., E. Masliah, J.C.P.-C., and S.A.L. wrote the paper.

The authors declare no conflict of interest.

[1]M.T., S.S.-B., X.Z., and P.X. contributed equally to this work.

[2]Present address: Covance, Inc., Princeton, NJ 08540-6233.

[3]To whom correspondence may be addressed. E-mail: pina-crespo@sbmri.org, heinemann@salk.edu, or slipton@sbmri.org.

This article contains supporting information online at www.pnas.org/lookup/suppl/doi:10.1073/pnas.1306832110/-/DCSupplemental.

glutamate sensor system (SuperGluSnFR) (17) to detect the local concentration of glutamate contiguous to astrocytes after exposure to Aβ peptides. To ensure the close apposition of the sensor probe (consisting of GluSnFR-transfected HEK 293 cells) to the astrocytes, the sensor cells were genetically engineered to coexpress neuroligin (18) (Fig. 1*A*). Unlike prior methods, the FRET GluSnFR technique allows unprecedented spatial and temporal resolution of local glutamate concentration on a subsecond timescale. This resolution was important for comparing extrasynaptic glutamate levels with the rapid electrophysiological effects of Aβ observed in subsequent patch-clamp recordings.

In mixed neuronal/astrocytic or astrocyte cultures, the addition of glutamate itself resulted in an increased normalized FRET ratio, with a standard curve revealing sensitivity in the dynamic range of 1 to ~100 μM, as reported previously (17), and similar to the glutamate sensitivity of native NMDARs (19). Within seconds of exposure to picomolar concentrations of naturally occurring Aβ prepared from human postmortem AD brain by a method modified from Selkoe and colleagues (1, 15, 20) or to nanomolar concentrations of oligomerized (but not monomeric) synthetic $Aβ_{1–42}$, we observed local increases in glutamate. Potentially, both neurons and glia contribute to glutamate release in our mixed cultures, so we also tested the response to Aβ in pure astrocyte cultures. In this case, the change in glutamate concentration was on the order of 30 μM and occurred in ~40% of the fields of astrocytes examined (Fig. 1 *B–D*; n = 370 responding cells quantified in 26 experiments). (For details of Aβ preparations, see *Materials and Methods* and Fig. S1.) Although naturally occurring Aβ yielded robust responses, synthetic $Aβ_{1–42}$ yielded significant increases in local glutamate with as little as 325 pM of an oligomerized preparation in both rat and human astrocyte cultures (Fig. S1*D*). HPLC analysis validated these results, revealing a small but significant rise in glutamate in the medium bathing the astrocytes after Aβ exposure (Fig. S1*E*). Depleting microglia from the astrocyte cultures using L-leucine methyl ester did not influence the level of glutamate (Fig. S1*F*), arguing for a direct effect of $Aβ_{1–42}$ on astrocytes under our conditions. Additionally, low-micromolar $Aβ_{25–35}$ also engendered local increases in glutamate release from astrocytes, as detected by the FRET GluSnFR technique (Fig. S1*G*). Control experiments showed that the transfected HEK cells did not respond to Aβ in the absence of astrocytes.

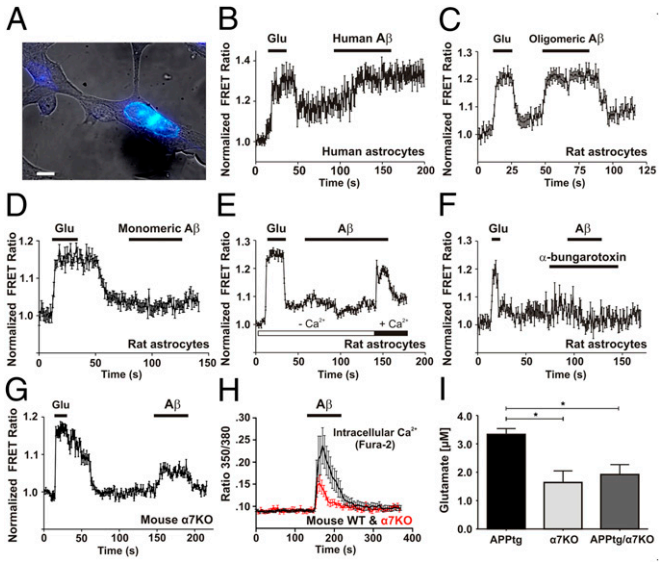

Fig. 1. Detection of astrocytic glutamate release after exposure to oligomeric Aβ. (*A*) Coculture of purified rat cortical astrocytes and HEK293T cells cotransfected with SuperGluSnFR and neuroligin to measure directly the time course of glutamate release. FRET fluorescence overlaid on bright-field imaging. (Scale bar: 10 μm.) (*B*) Human naturally occurring Aβ peptide (55 pM by ELISA; *Materials and Methods*) was applied to a coculture of purified human astrocytes and HEK cells expressing SuperGluSnFR, and the normalized FRET ratio was measured. The peak CFP/YFP ratio was divided by the baseline CFP/YFP ratio and was plotted after baseline normalization to 1. As measured with the FRET probe, Aβ induced glutamate (Glu) release from human astrocytes comparable to control applications of glutamate of ~30 μM. (*C*) Normalized FRET ratio reflecting glutamate release from purified rat astrocytes exposed to synthetic $Aβ_{1–42}$ (containing 250-nM oligomers; *Materials and Methods*). (*D*) Monomeric $Aβ_{1–42}$ (1 μM) did not induce glutamate release from purified astrocytes. Glutamate addition was used as a control. (*E*) Oligomerized $Aβ_{1–42}$ generated a robust FRET signal from astrocyte cultures in the presence but not the absence of extracellular Ca^{2+}. n = 24 cells analyzed in four experiments. (*F*) α-Bungarotoxin (100 nM), a selective antagonist of α7 nAChRs, abrogated oligomerized $Aβ_{1–42}$-induced glutamate release from rat astrocytes. n = 14 cells analyzed in three experiments. (*G*) Oligomerized $Aβ_{1–42}$-induced glutamate release also was largely eliminated in astrocytes from α7nAChR-knockout (α7KO) mice. n = 25 cells analyzed in four experiments. Values of the normalized FRET ratio in each panel are mean ± SEM. (*H*) By Fura-2 imaging, oligomerized $Aβ_{1–42}$ evoked a larger increase in intracellular Ca^{2+} in WT than in α7KO mouse astrocytes. n = 83 cells analyzed in three experiments. (*I*) In vivo microdialysis showed higher levels of extracellular glutamate in the hippocampus of 22- to 24-mo-old transgenic mice overexpressing human APP (hAPP tg) than in age-matched α7KO mice or in mice produced by crossing hAPP tg mice with α7KO mice (hAPP tg/α7KO). Data are shown as mean + SEM; n = 16; *$P \leq 0.05$ by t test with Bonferroni correction.

$Aβ_{1–42}$-Induced Glutamate Release from Astrocytes Requires Ca^{2+}. Because some forms of astroglial glutamate release are Ca^{2+} dependent (21), we asked whether oligomeric $Aβ_{1–42}$-induced glutamate release from astrocytes was dependent on Ca^{2+} influx. Indeed, when Ca^{2+} was omitted from the extracellular medium, Aβ failed to induce glutamate release, whereas the addition of Ca^{2+} immediately restored glutamate release (Fig. 1*E*). Absence of Ca^{2+} did not affect the sensitivity of glutamate sensor cells, because responses to exogenously applied glutamate were present in nominally Ca^{2+}-free solutions.

α7 Nicotinic Acetylcholine Receptors Mediate Aβ-Induced Glutamate Release from Astrocytes. $Aβ_{1–42}$ binds with high affinity to the α7 nicotinic acetylcholine receptor (α7nAChR) (22), a ligand-gated ion channel with high Ca^{2+} permeability that has been implicated in the pathology of AD (23). Because activation of α7nAChRs can increase intracellular Ca^{2+} ($[Ca^{2+}]_i$) in astrocytes (24), and glutamate release was calcium dependent, we next asked if α-bungarotoxin (α-Bgtx), a highly selective α7-antagonist, could inhibit Aβ-induced glutamate release from astrocytes. When oligomerized Aβ was applied to mouse astrocytes in the presence of 100 nM α-Bgtx, glutamate release was almost totally abrogated (Fig. 1*F*). Moreover, astrocytes obtained from α7nAChR-knockout mice released very little glutamate in response to Aβ, as monitored with the FRET GluSnFR probe (Fig. 1*G*). The decrease in Aβ-induced glutamate release was mirrored by a reduction in $[Ca^{2+}]_i$ in α7nAChR-knockout astrocytes as compared with WT (Fig. 1*H*). These findings support the notion that in addition to the reported inhibition of glutamate reuptake, Aβ induces release of glutamate from astrocytes, mediated at least in part by α7nAChRs. Aβ has been shown to bind to group I metabotropic glutamate receptors (25), but antagonists to these receptors manifested little or no effect on oligomeric Aβ-induced glutamate release in our system (Fig. S1*H*).

A caveat to these findings lies in the fact that astrocytic receptors and their pharmacological properties can change in culture. Hence, to vet our results showing extracellular glutamate accumulation in response to Aβ and its pharmacological properties in more intact systems, we performed experiments in vivo in animal models of AD during microdialysis. Using transgenic mice expressing human amyloid precursor protein (hAPP tg), we found basal glutamate levels were increased compared with nontransgenic littermates and that this increase was largely abrogated and was not statistically different from WT after crossing with α7nAChR-null mice (Fig. 1*I* and Fig. S1*I*). Our results

show that extracellular glutamate accumulates not only in culture but also in living brain in the presence of oligomerized Aβ in an α7nAChR-dependent manner (23). As a corollary, under our culture conditions as well as in vivo, the high density of transporters adjacent to synaptic sites would be expected to clear excessive glutamate released by Aβ away from synaptic receptors, although extrasynaptic receptors still might be activated (but see ref. 26). Hence, this premise was queried next.

Aβ Increases Extrasynaptic Glutamatergic Currents but Decreases Synaptic Currents in Rat Hippocampal Autaptic Cultures. Hippocampal microcultures contain a few or even a single neuron that synapses on itself to form an autapse; neurons are cultured in isolation or on a tiny bed of astrocytes (Fig. S2 *A* and *B*). This preparation allows rapid access of exogenous Aβ and applied drugs to neural tissue and also simultaneous recording of eNMDARs and sNMDARs with a single patch electrode. In hippocampal autaptic cultures, we found that picomolar naturally occurring Aβ-soluble oligomers, nanomolar oligomeric $Aβ_{1–42}$ (but not monomeric), or low-micromolar $Aβ_{25–35}$ (but not $Aβ_{35–25}$) induced a tonic inward current within tens of seconds of application in ∼55% of neurons (Fig. 2 *A*–*G*; $n = 90$). In excitatory neurons in the nominal absence of extracellular Mg^{2+}, the inward current was inhibited by the NMDAR antagonists (D-)-2-amino-5-phosphonovalerate (APV) or memantine (Fig. 2*F*) or by the combination of an NMDAR antagonist and an AMPA receptor (AMPAR) antagonist (Fig. 2 *A*–*C*). Prior work had shown that the tonic inward current in this preparation represents activation of extrasynaptic glutamate receptors (3, 5, 27, 28). To confirm this finding, we performed recordings after pharmacological isolation of extrasynaptic currents using the published protocol of first activating excitatory synaptic currents electrically followed by the addition of dizocilpine (MK-801) to block these synaptic responses (29) (Fig. S2 *C* and *D*). After isolating extrasynaptic currents in this manner, we found that $Aβ_{1–42}$ (containing 250-nM oligomers) resulted in increased eNMDAR activity similar to that seen with the application of low-micromolar glutamate (Fig. S2*E*).

When we studied autapses formed by inhibitory neurons, which release GABA rather than glutamate (Fig. S2*F*), we also observed a tonic inward current engendered by oligomerized $Aβ_{1–42}$ that was antagonized at least partially by 2,3-dihydroxy-6-nitro-7-sulfamoyl-benzo[f]quinoxaline (NBQX) plus memantine (Fig. 2*D*). This finding is consistent with the notion that glutamate was being released predominantly by astrocytes rather than neurons, because these inhibitory neurons do not release glutamate. If so, then the addition of α-Bgtx to these neuronal/astrocyte cultures should inhibit oligomerized $Aβ_{1–42}$-induced currents by inhibiting glutamate release from the astrocytes via blocking α7nAChRs. To test this premise in a manner that was pathophysiologically relevant to human AD, we used neurons and astrocytes derived from human induced pluripotent stem cells (hiPSCs). Consistent with the notion that astrocytic glutamate release is mediated by α7nAChRs, we found in this preparation that NMDAR antagonists inhibited oligomerized $Aβ_{1–42}$-induced currents, as did 100 nM α-Bgtx (Fig. S2 *G* and *H*).

Another important consideration is that memantine, like other NMDAR open-channel blockers, might block α7nAChR channels (30) and hence prevent release of glutamate from the astrocytes. We tested this possibility using our FRET probe and indeed found memantine produced a small decrement in glutamate release from astrocytes, but the effect did not reach statistical significance (Fig. S1*J*). Hence, this action could not account for the memantine effect, because substantial glutamate release remained. Nonetheless, this secondary effect of memantine on α7nAChRs potentially might contribute to the drug's ability to limit eNMDAR currents, because, at least in theory, glutamate release from astrocytes might be inhibited to a degree, in addition to memantine's direct blocking of eNMDAR-operated channels.

Importantly, in neurons in which synaptic currents in addition to extrasynaptic responses were monitored quantitatively after the addition of TTX, we found a decrement in mEPSC frequency and a smaller or no decline in mEPSC amplitude within minutes of Aβ exposure (Fig. 2 *E* and *H*–*M*). The significant decrease in mEPSC frequency suggested a presynaptic deficit, but functional loss of synapses in response to oligomeric Aβ under these conditions was possible also. We knew these autaptic cells were well clamped, because the miniature synaptic currents reversed at or near 0 mV, as expected for excitatory cation-mediated responses under our conditions. Interestingly, in neurons that did not manifest any extrasynaptic glutamatergic current in response to Aβ, we did not observe a subsequent decrease in mEPSC frequency. Furthermore, depletion of astrocytes from the cultures largely abrogated these effects of oligomeric Aβ (Fig. S2*I*), even though excitatory neurons have been shown to release synaptic glutamate in response to Aβ (31). The fact that the Aβ-induced current was greatly abated in

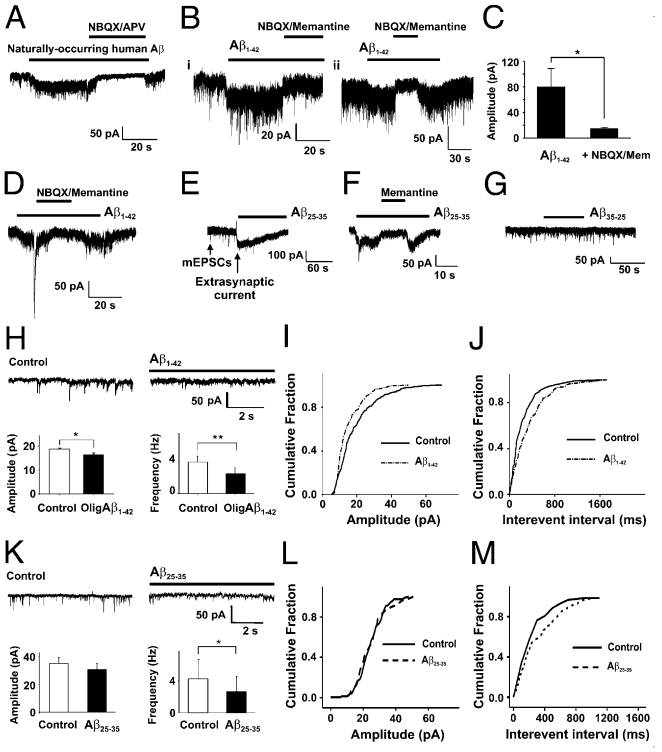

Fig. 2. Application of various Aβ preparations (naturally occurring human Aβ, oligomeric synthetic $Aβ_{1–42}$, or $Aβ_{25–35}$) to autaptic hippocampal neuronal cultures induces extrasynaptic inward currents and decreases mEPSC frequency in a glutamate receptor antagonist-sensitive manner. (*A*) Naturally occurring human Aβ (55 pM) induced extrasynaptic current in neurons that was inhibited by glutamate receptor antagonists NBQX (10 μM) and D-APV (100 μM). (*B*) $Aβ_{1–42}$ (containing 500-nM oligomers) induced extrasynaptic current in glutamatergic autaptic neurons, which could be largely inhibited by NBQX (10 μM) plus memantine (10 μM). (*C*) NBQX (10 μM) plus memantine (10 μM) significantly reduced the amplitude of $Aβ_{1–42}$-induced extrasynaptic currents. Data are shown as mean + SEM; $n = 8$; $^*P < 0.05$ by *t* test. (*D*) Oligomerized $Aβ_{1–42}$ also induced extrasynaptic current in GABAergic autaptic neurons. Large, transient inward current represents an inhibitory postsynaptic current. (*E*–*G*) Application of $Aβ_{25–35}$ (10 μM), but not $Aβ_{35–25}$, also induced inward extrasynaptic current sensitive to memantine with a mean amplitude of 45.9 ± 11.2 pA in 42% of recorded cells. (*H*) In well space-clamped autapses, both mEPSC amplitude and mEPSC frequency were decreased significantly after exposure to oligomerized $Aβ_{1–42}$. $n = 9$; $^*P < 0.05$, $^{**}P < 0.01$ by *t* test. (*I*) Representative cumulative probability graphs of mEPSC amplitudes. (*J*) Representative cumulative probability graphs of mEPSC interevent intervals. (*K*) Amplitude of mEPSC was not altered but frequency was decreased significantly after $Aβ_{25–25}$ exposure. $n = 5$; $^*P < 0.05$ by *t* test. (*L*) Representative cumulative probability graphs of mEPSC amplitudes. (*M*) Representative cumulative probability graphs of mEPSC interevent intervals.

the absence of astrocytes also was consistent with the notion that the predominant effect on extrasynaptic current observed here did not result from direct action of Aβ on neuronal NMDARs. Although these experiments do not rule out a direct effect of Aβ on neurons, they do indicate that the major effects observed under our conditions were dependent on the presence of astrocytes.

Additionally, in the absence of TTX we observed that cells responding to Aβ with an inward extrasynaptic current manifested subsequent evoked EPSCs with smaller AMPAR- and NMDAR-mediated components than in control (Fig. S2*J*). This result might reflect the development of silent synapses, endocytosis of AMPARs, or sNMDAR depletion resulting from EphB2 binding of exogenous Aβ, as previously reported (10, 32, 33). However, coupled with the very significant decrease in mEPSC frequency that we observed in the hippocampal autaptic preparation, our results also are consistent with the notion of rapid compromise or functional loss of the synapse after Aβ exposure. Hence, we further investigated this possibility next.

Aβ Activation of eNMDARs Increases Neuronal Ca^{2+} and NO. Using Fura-2, we performed Ca^{2+} imaging experiments in mixed neuronal/astrocytic cultures after exposure to Aβ. We observed an increase in neuronal Ca^{2+} in response to nanomolar oligomerized $A\beta_{1-42}$ or micromolar $A\beta_{25-35}$ (but not to nonoligomerized $A\beta_{1-42}$ or $A\beta_{35-25}$) that was largely abrogated by 5–10 μM memantine and its more potent adamantane nitrate derivative, NitroMemantine (Fig. 3 *A* and *B* and Fig. S3 *A*–*C*) (34). At this concentration in this preparation, we previously have shown that memantine and NitroMemantine preferentially block eNMDARs while relatively sparing sNMDARs (3, 28). As a control, this effect of Aβ also was largely blocked in cultures depleted of astrocytes. Taken together with the foregoing results, these findings are consistent with the notion that Aβ induced release of glutamate from astrocytes, which in turn activated neuronal eNMDARs.

Excessive influx of Ca^{2+} via NMDARs activates neuronal nitric oxide synthase, which generates toxic levels of NO (35, 36). NO has been shown to contribute to synaptic spine loss after Aβ exposure, at least in part via mitochondrial actions of S-nitrosylated dynamin-related protein 1 (Drp1) after transnitrosylation from cyclin-dependent kinase 5 (Cdk5) enzyme (37, 38). Accordingly, in our cultures, in addition to a rise in neuronal Ca^{2+} levels, Aβ induced an increase in NO, as monitored with diaminofluorescein (DAF) fluorescence imaging (38, 39). Both memantine and NitroMemantine prevented this Aβ-induced increase in NO (Fig. 3*C* and Fig. S3*B*). Notably, NitroMemantine was significantly more effective than memantine in abrogating the increase in Ca^{2+} and toxic NO response, consistent with its more effective tonic blockade of eNMDARs, as previously suggested electrophysiologically (34). Confirming the involvement of eNMDARs in this process, we also found similar changes in Ca^{2+} and NO in response to oligomeric Aβ after pharmacological isolation of extrasynaptic currents using the published protocol of activating excitatory synaptic currents (by antagonizing inhibitory currents with the GABA antagonist bicuculline) followed by the addition of MK-801 to block the excitatory synaptic responses (Fig. S3 *D* and *E*) (3, 27, 28).

Extrasynaptic NMDARs Mediate Aβ-Induced Synaptic Depression in Hippocampal Slices. Previously, Selkoe and colleagues demonstrated that soluble oligomeric Aβ depressed long-term potentiation induced by high-frequency stimulation while enhancing long-term depression induced by electrical (low-frequency) stimulation (1, 15, 20, 40). Considering that accumulation of extracellular glutamate induced by high levels of oligomeric Aβ, as observed here, might underlie changes in synaptic function and plasticity, we next investigated the effect of Aβ on synaptic depression. To do so, we studied synaptic transmission at the Schaffer collateral–CA1 pathway of the hippocampus using electrophysiological recording of synaptic field potentials in acute hippocampal slices. We observed that as little as 50 nM oligomeric (but not 1 μM monomeric) $A\beta_{1-42}$ induced a gradual depression of field excitatory postsynaptic potentials (fEPSPs), outlasting the application of Aβ (Fig. 4*A*; $n = 12$). Although the input–output relationship also was affected by oligomeric $A\beta_{1-42}$, paired-pulse facilitation remained largely unaffected (Fig. 4 *B* and *C*).

In some ways, this effect of Aβ was reminiscent of chemical long-term depression, whereby glutamate induces synaptic depression that is modulated, at least in part, by eNMDARs (41–43). Therefore, we asked whether Aβ-induced synaptic depression might be mediated through eNMDARs by applying memantine, which we have shown at low-micromolar concentrations blocks eNMDARs to a relatively greater degree than sNMDARs (3, 28). We found that 10 μM memantine blocked induction of synaptic depression by 50 nM $A\beta_{1-42}$ (Fig. 4*D*; $n = 4$). Moreover, 500 nM $A\beta_{25-35}$ (but not $A\beta_{35-25}$) induced synaptic depression that was inhibited by 10 μM memantine or 5 μM NitroMemantine (Fig. S4 *A* and *B*). This latter finding is consistent with the greater potency of NitroMemantine at eNMDARs over memantine (Fig. 3 *B* and *C* and Fig. S3).

Next, we hypothesized that if eNMDARs indeed contributed to Aβ-induced synaptic depression, then activation of extrasynaptic receptors by exogenous NMDA (5–50 μM) should recapitulate the synaptic depression caused by Aβ and should be inhibited by low-micromolar memantine or NitroMemantine; in fact, we found this to be the case (Fig. S4*C*).

Increased Tonic eNMDAR-Mediated Activity in AD Brain Slices. Given the evidence for activation of eNMDARs after acute application of Aβ, one might expect persistent eNMDAR-mediated activity from long-term accumulation of oligomerized Aβ in the AD brain. Hence, we asked if eNMDARs were tonically overstimulated in transgenic AD models of Aβ overexpression (33). Indeed, compared with WT littermate controls, we found a significant increase in basal inward current in neurons from the CA1 region of hippocampal slices prepared from hAPP-J20 tg mice in

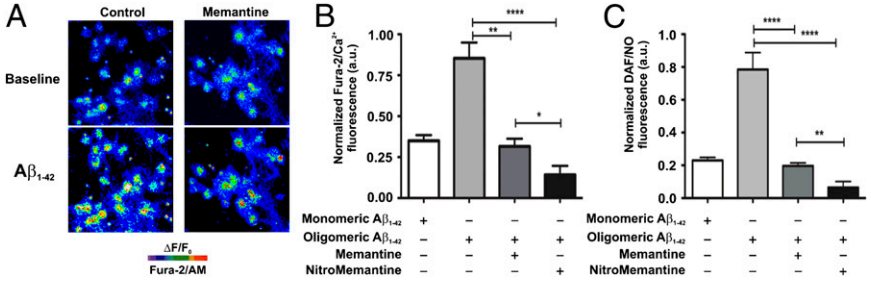

Fig. 3. Memantine and NitroMemantine inhibit Aβ-induced $[Ca^{2+}]_i$ increase and NO generation in cultured rat primary cortical neurons. (*A*) Images of cells before (Baseline) and after exposure to $A\beta_{1-42}$ (250-nM oligomers) with and without treatment with memantine. Colored bar indicates neuronal Ca^{2+} levels ($[Ca^{2+}]_i$) determined with Fura-2/AM. (*B* and *C*) Change in Fura-2 and DAF fluorescence intensity with the addition of monomeric (1 μM) or oligomeric $A\beta_{1-42}$ (250 nM) in the presence and absence of memantine or NitroMemantine (5 μM). Values for the change in fluorescence intensity were calculated as change in intensity divided by baseline intensity ($\Delta F/F_0$) and were plotted as a fraction of 1. Values are mean + SEM for all panels. $^*P < 0.05$, $^{**}P < 0.01$, $^{***}P < 0.001$; $n \geq 40$ neurons for each condition. a.u., arbitrary units.

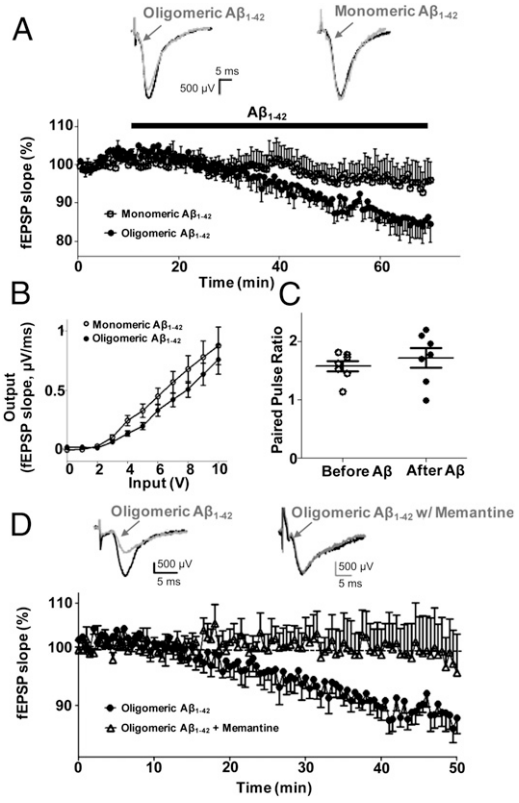

Fig. 4. Soluble oligomeric $A\beta_{1-42}$ induces synaptic depression in hippocampal slices. (*A*) fEPSPs were gradually depressed after slices were perfused with 50 nM oligomeric $A\beta_{1-42}$. In contrast, monomeric $A\beta_{1-42}$ (1 μM) had no effect on fEPSPs. $n = 12$. (*B*) Effect of oligomeric vs. monomeric $A\beta_{1-42}$ on input–output curves. $n = 12$. (*C*) Effect of oligomeric vs. monomeric $A\beta_{1-42}$ on paired-pulse ratio. $n = 12$. (*D*) Memantine inhibited oligomeric $A\beta_{1-42}$-induced synaptic depression. $n = 11$.

nominal absence of extracellular Mg^{2+} (Fig. 5; $n = 15$, $P < 0.01$). Pharmacological inhibition by the AMPAR antagonist 6-cyano-7-nitroquinoxaline-2,3-dione (CNQX) plus the NMDAR antagonist 3-[(R)-2-carboxypiperazin-4-yl]-propyl-1-phosphonic acid (CPP) showed that this basal current was induced by glutamate (Fig. 5 *A*, *B*, and *E* and Fig. S4*D*). Moreover, application of 100 nM α-Bgtx largely abrogated the basal current, consistent with the notion that α7nAChRs were mediating release of glutamate in the slices, as encountered earlier in our culture and in vivo AD models. Additionally, CNQX plus CPP blocked mEPSCs in these slices, indicating the glutamatergic nature of these synaptic currents (Fig. 5 *A*–*D*).

Although the small basal glutamatergic currents in some control WT slices (e.g., Fig. 5*A*) could be ascribed to leakage or damage, other control slices manifested virtually no basal current (Fig. 5*F*). Moreover, memantine (10 μM), which is known to inhibit eNMDARs preferentially over sNMDARs (3, 28), substantially blocked the basal current in hAPP-J20 slices (Fig. 5 *G* and *H*) but had little or no effect on mEPSC amplitude or frequency in WT slices even with incubation periods of more than 1 h (Fig. 5*I*). In contrast, after ∼30 min of perfusion with memantine, mEPSCs frequency increased but amplitude and kinetics remained relatively unaffected in hAPP-J20 slices (Fig. 5*J*). These findings are consistent with the notion that the loss of synaptic function observed with chronic exposure to Aβ might be partially reversible on a relatively short time scale if excessive eNMDAR activity were inhibited, in this case by memantine.

To obtain evidence independent of memantine that the basal current was indeed mediated by eNMDAR activation, we took advantage of the recent report that glycine is the predominant coagonist of eNMDARs. Thus, by degrading glycine in slice preparations, the enzyme glycine oxidase (GO) can inhibit eNMDAR-mediated responses. In contrast, enzymes that degrade D-serine, such as D-amino acid oxidase (DAAO) or D-serine deaminase (DsdA), can inhibit sNMDAR-mediated responses (44, 45). We used this approach to provide further proof that the basal inward current seen in the hAPP-J20 slices (and associated with our measurement of extracellular glutamate in these mice by HPLC) is caused by eNMDAR activity, because GO but not DAAO largely blocked this current (Fig. S5 *A* and *B*).

Next, we studied mEPSCs in hippocampal slices from hAPP-J20 and WT littermates in more detail. We observed a significant decrease in frequency ($P < 0.01$), a small but insignificant decrease in amplitude, and no change in kinetics of mEPSCs in hAPP-J20 slices compared with WT (Fig. 5 *K*–*O*; $n = 12$).

Extrasynaptic NMDARs Mediate Aβ-Induced Molecular Cascades Leading to Synaptic Spine Loss. We sought a heuristic explanation for the decrease in mEPSC frequency that occurred in response to Aβ-induced eNMDAR activity in hippocampal autapses and in hAPP-J20 hippocampal slices, as well as for the partial recovery of mEPSC frequency in hAPP-J20 tg slices treated with memantine. One possibility is that the decrease in mEPSC frequency reflects initial synaptic dysfunction that subsequently leads to synapse loss. We reasoned that, if the initial decrease in mEPSC frequency induced by eNMDAR activity truly represented the initial phase of synaptic damage, then the molecular pathway(s) underlying this damage should be engaged early on and that pharmacological blockade of eNMDARs should inhibit these molecular pathways and give protection from subsequent morphological loss of dendritic spines. Such spine loss has been observed to occur ∼16 h after exposure to oligomerized Aβ (1), although an initial decrease in spine volume has been reported as early as 10 min (10). Here, we found that treatment of our mixed neuronal/glial cultures with the standard pharmacological protocol to activate eNMDARs selectively after blocking sNMDARs (using bicuculline exposure followed by MK-801, washout, and then exposure to low concentrations of NMDA) (3, 27, 28) triggered an increase in tau and hyperphosphorylated tau and in caspase-3 activation (Fig. 6 *A* and *C*). When the cultures were exposed to oligomerized Aβ rather than low-dose NMDA, phospho-tau increased more dramatically than tau (Fig. 6*B*). Importantly, these same pathways involving phospho-tau and caspase-3 previously were shown to be involved in oligomeric Aβ-induced abnormal excitability and synaptic spine loss (10, 11, 14, 46–56). For example, the relatively specific inhibitor of caspase-3 activity, z-DEVD-fmk, blocks a pathway leading to dendritic spine shrinkage via activation of calcineurin, which results in dephosphorylation and internalization of synaptic AMPARs (56). As would be expected for a mechanism involving eNMDAR activation, this effect of Aβ was inhibited by memantine and to an even greater degree by NitroMemantine (Fig. 6*B*). In contrast to eNMDARs, selective pharmacological activation of sNMDARs led to a decrease in tau phosphorylation and caspase-3 activation (Fig. 6 *A* and *C*).

To assess the contribution of eNMDAR activity to Aβ-induced synapse loss, we next exposed hippocampal slices to oligomerized Aβ and then treated them with memantine or its improved derivative NitroMemantine to block eNMDARs selectively while relatively sparing sNMDARs (3, 28). In fact, at equimolar concentrations NitroMemantine (34) is more effective than memantine not only in blocking eNMDAR activity but also in sparing synaptic activity (Fig. 3 *B* and *C*, Fig. S3, and Fig. S4 *A*, *B*, and *E*). We found that treatment with these eNMDAR-selective antagonists ameliorated the effect of Aβ on synaptic loss, with NitroMemantine manifesting a larger and more significant protective effect than memantine, as monitored morphologically in YFP-labeled dendritic spines (Fig. 6 *D* and *E*). To confirm that this protective effect was mediated by eNMDARs, we used a second approach to inhibit eNMDARs vs. sNMDARs by bathing hippocampal slices in glycine and D-serine–degrading enzymes (44, 45, 57). We found that only inhibition of eNMDARs with

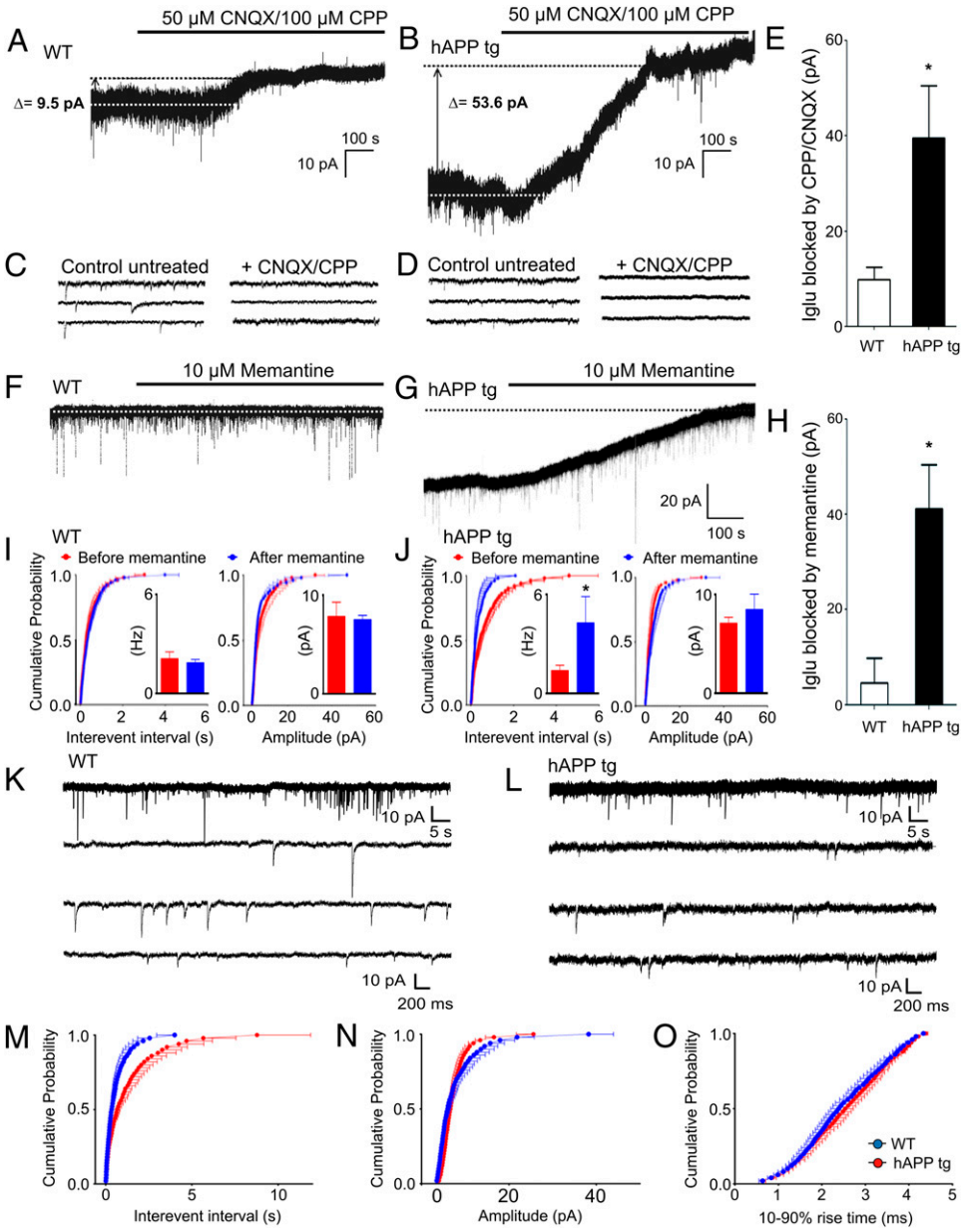

Fig. 5. NMDAR antagonists inhibit relatively large basal glutamatergic currents (Iglu) observed in hippocampal slices from hAPP-J20 tg mice but not from WT littermates during whole-cell recording. (*A*) In WT mice, 100 μM CPP/50 μM CNQX blocked a small background Iglu of 9.5 pA observed at a holding potential (V_h) = −70 mV. (*B*) In an APP-J20 tg littermate, 100 μM CPP/50 μM CNQX blocked a larger basal Iglu of 53.6 pA at Vh = −70 mV. (*C* and *D*) In slices from both WT and J20 transgenic littermates, 100 μM CPP/50 μM CNQX also blocked mEPSCs. (*Left*) Untreated control. (*Right*) Drug treated. (*E*) At Vh = −70 mV, 100 μM CPP/50 μM CNQX inhibited a mean Iglu of 9.9 pA in WT littermates and 39.3 pA in transgenic littermates. $n = 8$; $^*P < 0.01$. (*F*) In another WT littermate, there was little if any basal Iglu, and perfusion with 10 μM memantine manifested no effect at Vh = −70 mV. (*G*) In a J20 transgenic littermate, perfusion with 10 μM memantine blocked a background Iglu of 46.5 pA at Vh = −70 mV. (*H*) Memantine blocked a mean basal Iglu of 4.7 pA in hippocampal slices from WT mice but 41.2 pA in J20 transgenic littermates. $n = 7$; $^*P < 0.01$. (*I*) In WT slices, 10 μM memantine manifested little or no effect on the frequency or amplitude of mEPSCs, even with very prolonged incubation times on the order of hours. (*J*) In slices from hAPP-J20 tg littermates, perfusion with 10 μM memantine for periods ≥30 min resulted in increased frequency of mEPSCs, as reflected by a leftward shift in the interevent interval in the cumulative probability curve, but had only minor or no effect on amplitude. $n = 7$ slices for *I* and *J*. (*Insets*) Histograms of frequency and amplitude. Data are shown as mean + SEM; $^*P < 0.01$. (*K*) mEPSCs recorded from CA1 neurons in WT mice in the presence of 1 μM TTX and 50 μM picrotoxin (Vh = −70 mV). (*L*) mEPSCs recorded in hAPP-J20 tg mice under similar conditions. (*M*) Cumulative probability showing decreased mEPSC frequency in J20 transgenic vs. WT mice, as reflected by an increase in the interevent interval. $n = 12$; $P < 0.00001$ for mEPSC frequency by Kolmogorov–Smirnov test. The noise level was greater in J20 than in WT mice because of the presence of increased basal current from extrasynaptic glutamate. To avoid bias due to this noise level, the analysis of mEPSC frequency used the same event threshold for both sets of data. (*N* and *O*) Cumulative probability of mEPSC amplitude and kinetics in hAPP-J20 tg vs. WT mice. $n = 12$.

glycine oxidase significantly protected from spine loss induced by oligomerized Aβ (Fig. S5*C*). Taken together, these results suggest that early events associated with hyperactivation of eNMDARs by Aβ indeed may be linked to the subsequent loss of synapses in AD.

Effect of Inhibiting eNMDARs in Vivo in an AD Transgenic Mouse Model. To test further the effect of inhibiting eNMDARs relative to sNMDARs with memantine and NitroMemantine, we treated the triple transgenic (3× tg) AD mouse model for 3 mo starting at 6 mo of age. This mouse model of AD manifests early synaptic

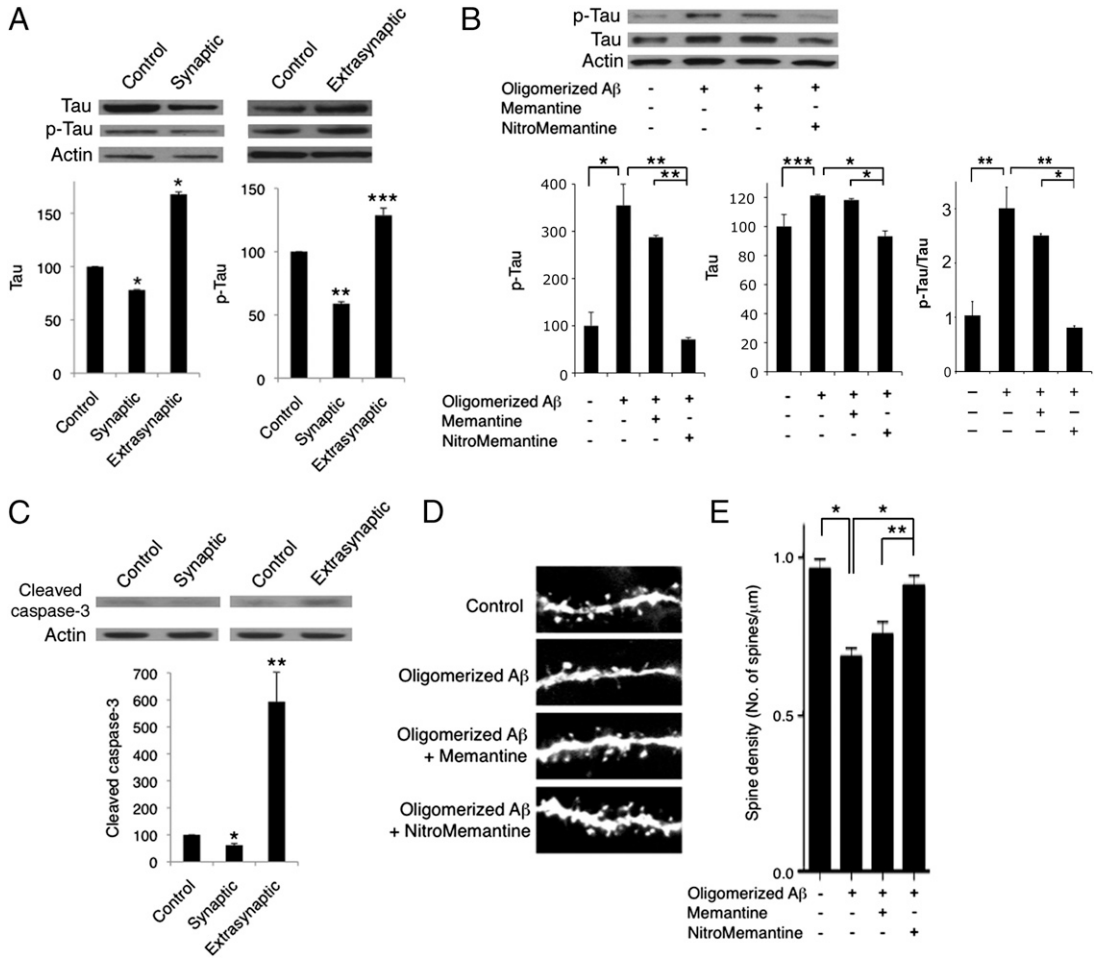

Fig. 6. eNMDAR activity triggers the molecular cascade and dendritic spine loss associated with synaptic damage induced by Aβ peptide. (*A*) Western blots showing that synaptic activity reduced and extrasynaptic NMDAR activity increased the levels of tau and phospho-tau (p-tau) in mixed neuronal/glial cultures. Quantification is shown relative to the level of actin as the loading control. $*P < 0.05$, $**P < 0.01$, and $***P < 0.001$ by ANOVA. (*B*) Blockade of extrasynaptic relative to synaptic NMDAR activity using memantine or NitroMemantine (5 μM each) decreased p-tau and to a lesser degree total tau levels after exposure to oligomerized $A\beta_{1-42}$. $n = 3$. The effect of NitroMemantine was greater than that of memantine. Quantification is shown relative to actin. $*P < 0.01$, $**P < 0.001$, $***P < 0.05$ by ANOVA. (*C*) Western blots showing that synaptic activity reduced and extrasynaptic NMDAR activity increased cleaved caspase-3. Quantification is shown relative to actin. $*P < 0.01$, $**P < 0.001$ by ANOVA. (*D* and *E*) Blockade of eNMDAR activity by NitroMemantine abrogated dendritic spine loss mediated by oligomerized Aβ in hippocampal slices to a greater degree than memantine. Hippocampal neurons from YFP-transgenic mice were exposed for 7 d to control or synthetic $A\beta_{1-42}$ (500-nM oligomers) in the presence or absence of memantine or NitroMemantine (each at 10 μM). $n > 12$ for each condition; $*P < 0.001$, $**P < 0.05$. Histograms for all panels show mean + SEM.

dysfunction and cognitive deficits in the presence of soluble Aβ and abnormal tau protein before the formation of frank amyloid plaques and tau tangles (58). We used this mouse because we wanted to analyze the effect of soluble oligomeric Aβ, rather than plaques and tangles, and, unlike other AD mouse models, there were few if any plaques or tangles when the mice were treated. Moreover, this mouse model displayed only very mild loss of neurons in the neocortex and hippocampus, despite a dramatic loss of synapses. Hence, neuronal loss could not account for the decrease in synapses. By quantitative confocal immunofluorescence microscopy in both the cortex and hippocampus, after treatment we observed a significant increase in synaptic and dendritic density by synaptophysin and microtubule-associated protein 2 (MAP2) staining, respectively (Fig. 7 *A–E*). As in the hippocampal slice preparation, NitroMemantine demonstrated an effect superior to that of memantine. Additionally, in behavioral studies of hippocampal function, NitroMemantine-treated (but not memantine-treated) 3× tg AD mice displayed significantly improved function on the location-novelty recognition test (Fig. 7*F*).

Discussion

Recent studies suggest that eNMDAR activity inhibits neuroprotective pathways and signals neuronal injury, whereas sNMDAR activity stimulates neuroprotective transcriptional and antioxidant pathways (6). Although this paradigm first was demonstrated for ischemic brain disease, accumulating evidence suggests that it also is true for neurodegenerative disorders involving protein misfolding, such as Huntington disease (3, 4) and AD (7, 8, 59, 60). Additionally, linking this dichotomy of eNMDAR vs. sNMDAR activation to synaptic integrity, we and others previously have shown that low levels of glutamate or endogenous synaptic activity may enhance dendritic spine growth (61, 62). Moreover, normal endogenous levels of Aβ may increase mEPSC frequency, reflecting increased physiological synaptic glutamate release (31). In contrast, excessive glutamate, leading to eNMDAR activation, can precipitate loss of dendrites and spines (6, 61). Here we demonstrate that soluble oligomeric Aβ engages astrocytic α7nAChRs to induce glutamate release from astrocytes, with local levels in the extracellular space approaching tens of micromolar. In turn, resulting neuronal eNMDAR activation leads to both functional and molecular changes, heralding synaptic

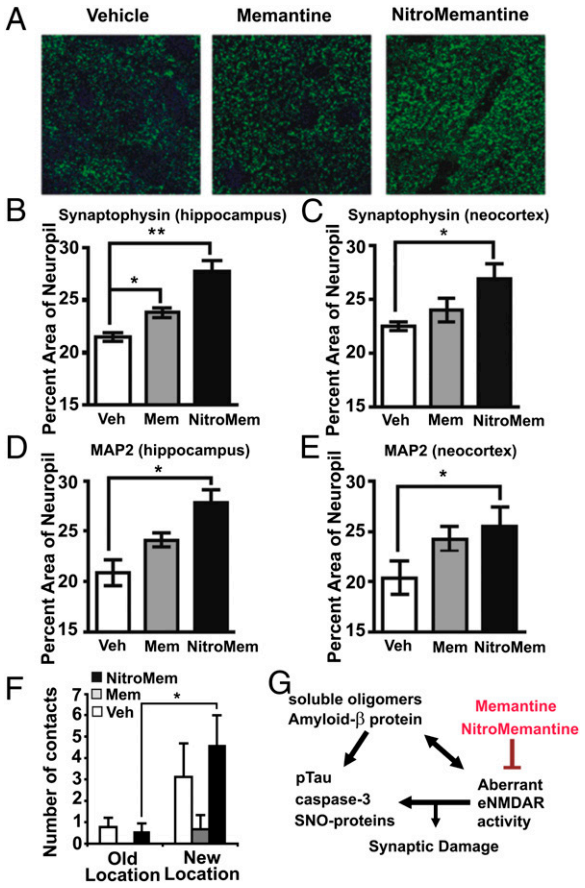

Fig. 7. Immunocytochemical and neurobehavioral analysis of AD transgenic mice plus schematic of Aβ effects on synapses. (*A–E*) Quantitative confocal fluorescence imaging in hippocampus and frontal cortex of synaptic marker synaptophysin (representative images from hippocampus are shown in *A*) and dendritic marker MAP2 in 3× tg AD mice treated with vehicle, memantine, or NitroMemantine. $n = 9$; $^{*}P < 0.05$, $^{**}P < 0.01$. (*F*) Improvement in neurobehavioral assessment of hippocampal function on the location novelty recognition test [or novel location (NL)] in 9-mo-old 3× tg AD mice after a 3-mo treatment with NitroMemantine compared with the effect of memantine or vehicle-treated control. In this task, the number of contacts with the object in the final familiarization trial before the object was moved (Old Location) and the number of contacts made after the same object was moved (New Location) were monitored. There were no group differences in initial contacts with the three objects, and all were explored between five and seven times during the first familiarization trial. Only the NitroMemantine-treated group manifested a significant increase in their ability to detect spatial change, as monitored by the increased number of contacts with the object after it was moved. $^{*}P < 0.03$ by ANOVA; $n = 24$. (*G*) Schematic diagram showing influence of eNMDAR activity on Aβ-induced synaptic damage in AD.

damage. Strikingly, these changes occur within minutes of Aβ-induced eNMDAR activation, before actual histological loss of the synapse, which can take several hours to observe (1). Our finding that α7nAChRs play a significant role in Aβ-induced glutamate release from astrocytes is in agreement with prior studies showing that α7nAChRs represent a binding site for Aβ (22). Moreover, the present study links the cholinergic and glutamatergic systems in AD and as such may lead to additional strategies for therapeutic intervention. Importantly, our findings also indicate that Aβ-induced neuronal synaptic loss in AD may, in large part, be dependent on non–cell-autonomous actions of oligomeric Aβ on glial cells (in our case astrocytes), although the involvement of microglia also has been implicated in other studies.

Intriguingly, we found that Aβ induced a tonic glutamatergic current in hippocampal neurons. This extrasynaptic inward current, at least in part mediated by astrocytic glutamate release and subsequent activation of eNMDARs, was followed by a decrement in mEPSC frequency. We reasoned that the decrease in mEPSC frequency that we observed with Aβ exposure in both hippocampal autapses and slices might represent initial synaptic dysfunction, which only later was followed by frank synapse loss. Additionally, eNMDAR-mediated increases in NO generation, tau protein, tau hyperphosphorylation, and caspase-3 activity that we found in response to oligomerized Aβ argue that these early molecular events presage the loss of synapses that we observed hours later. Prior experiments had shown that after acute exposure to Aβ (10, 32, 63), other synaptic events also may occur, such as internalization via endocytosis of postsynaptic receptors to account for a decrease in mEPSC amplitude. However, this mechanism alone would not adequately account for the decrease in mEPSC frequency (but not amplitude) that we observed after chronic Aβ exposure in the hAPP-J20 hippocampus and that was reversed, at least partially, with prolonged memantine treatment. Importantly, the concentration of memantine we used correlates well with the dosage approved by the Food and Drug Administration for treatment of moderate-to-severe AD in humans (3, 28), and these results may account, at least in part, for the drug's beneficial albeit modest effect.

Although under our conditions memantine and NitroMemantine inhibit sNMDARs relatively less than eNMDARs (3, 28), it might be argued that the drugs' protective effect on synapses actually was mediated via their more minor sNMDAR effects rather than by their major action on eNMDARs. However, we believe that this possibility is highly unlikely, given that Aβ exposure decreased mEPSCs, reflecting in part less sNMDAR activity, whereas the presence of memantine and NitroMemantine preserved and actually increased this activity. Hence, it would appear that, under the conditions in which memantine and NitroMemantine protected synapses from Aβ-induced damage, the relatively minor inhibition of sNMDARs by these drugs could not have been responsible. Therefore, we conclude that inhibition of excessive eNMDAR activity likely was responsible for the beneficial effect on synaptic protection. The corollary of this conclusion is that Aβ-induced eNMDAR activity was in large part responsible for synaptic dysfunction/loss, because we found that inhibition of this aberrant activity protected the structure and function of the synapses.

Concerning the mechanism of Aβ-induced eNMDAR activity on synaptic damage, the pharmacological data presented here and elsewhere (37, 38) indicate that tau phosphorylation, caspase-3 activation, and NO-mediated events [formation of S-nitrosylated (SNO)-Drp1 and SNO-Cdk5] all appear to be largely mediated by eNMDARs. Because these events occur rapidly, within minutes of eNMDAR activation, the early changes that we observed in synaptic function could serve as the harbinger of subsequent synaptic damage and loss. Critically, our empirical data indicate that these untoward effects on synaptic form and function are reversible, at least in part, after eNMDAR inhibition (e.g., by memantine and even more effectively by NitroMemantine) in both hippocampal slices and in vivo rodent models of AD.

Previously, Aβ was thought to injure the synapse directly, and changes in glutamate receptors and synapses were considered readouts of this damage. Here, we present evidence that glutamate itself, after Aβ-induced release from astrocytes, is responsible, at least in part, for triggering synaptic loss. Additionally, the effect of eNMDAR vs. sNMDAR activity on Aβ production and oligomerization (7, 8, 59, 60) could produce a positive feedback loop whereby oligomerized Aβ induces eNMDAR activity, as shown here, and eNMDAR activity also triggers toxic Aβ generation (Fig. 7*G*). These findings have considerable influence on our view of potential disease-modifying drugs for AD, implying that synapse protection may be achieved by eNMDAR antagonists that are sufficiently potent to protect but also are gentle enough to allow normal synaptic transmission and neurobehavioral improvement, as we observed here with the newer NitroMemantine drug both in vitro and in vivo.

Materials and Methods

Cell Cultures. Mixed neuronal/glial rat cerebrocortical cultures and purified rat, mouse, and human astrocytes were prepared following standard protocols with some modifications (37). For studying autapses, microisland rat hippocampal cultures were prepared as previously described (*SI Materials and Methods*) (28).

Generation of hiPSC-Derived Neurons from Dermal Fibroblasts. To generate hiPSCs from human dermal fibroblasts, we used an integration-free reprogramming method that used electroporation of three episomal expression vectors collectively encoding six reprogramming factors, namely OCT3/4, SRY-box containing gene 2 (SOX2), Kruppel-like factor 4 (KLF4), L-MYC, LYN28, and p53-shRNA) (64). hiPSC colonies were maintained on mouse embryonic fibroblast feeders and were validated for pluripotency, trilineage differentiation capability, and karyotypic stability as previously described (65) (*SI Materials and Methods*).

Glutamate FRET Imaging. Using FRET microscopy of the SuperGluSnFR probe (17), we monitored glutamate release from mixed neuronal/glial and pure astrocyte cultures (*SI Materials and Methods*).

Glycine and D-Serine Degradative Enzymes. Recombinant glycine oxidase (GO) and D-serine deaminase were purified as described (57). D-Amino acid oxidase) was purchased from a commercial source (Calzyme). All enzymes were kept frozen and were dissolved immediately before use.

Aβ Preparations. Human synthetic $A\beta_{1-42}$ (GenicBio or Anaspec) was dissolved following established procedures. Naturally occurring soluble Aβ dimers and trimers were prepared by size-exclusion chromatography from postmortem human AD cortex, with minor modifications of the procedure described previously (1, 15, 20, 40). By ELISA, this preparation contained 220 pM of Aβ before 1:4 dilution for use in experiments at a final concentration of 55 pM. For all Aβ preparations, concentration and quality were assessed by ELISA and Western blot analysis (*SI Materials and Methods*).

Measuring $A\beta_{1-42}$ Oligomer Concentration by Dynamic Light Scattering. The $A\beta_{1-42}$ oligomeric concentration was analyzed as reported previously (*SI Materials and Methods*) (66).

Electrophysiology. For hippocampal autaptic cultures, whole-cell recordings were performed on single neurons located on microislands of one or more astrocytes. Recordings were performed on 14–26 d in vitro cultures at room temperature using a patch-clamp amplifier (Axopatch 200B or MultiClamp 700A; Molecular Devices). Drugs were administered via a fast valve-controlled perfusion system (Lee Company). All antagonists were purchased from Tocris Bioscience unless otherwise noted. The NitroMemantine derivative used in these studies is the lead drug candidate designated YQW-036/NMI-6979 (34). For data acquisition and analysis, signals were filtered, digitized, and stored in a computer (Dell) using PClamp v.10 software (Axon Instruments). Display and analysis of data distributions were carried out using a statistical software package (Origin 7, OriginLab Corp.) (*SI Materials and Methods*).

$[NO]_i$ and $[Ca^{2+}]_i$ Measurements. Intracellular nitric oxide $[NO]_i$ and calcium $[Ca^{2+}]_i$ concentrations in cells in primary cultures were measured using DAF FM diacetate (2.5 μM) and Fura-2/AM (4 μM), respectively (*SI Materials and Methods*).

Pharmacological Isolation of eNMDARs from sNMDARs. To assess the effect of eNMDARs selectively, we initially activated sNMDARs by a brief (7–10 min) application of bicuculline (50 μM) to block inhibitory transmission and then blocked the sNMDARs with the long-lasting NMDAR inhibitor MK-801 (10 μM), as previously described (3, 5, 28). After bicuculline and MK-801 were washed out from the dish, NMDA or Aβ (to release glutamate from astrocytes) was added to elicit eNMDAR-dependent signaling.

Dendritic Spine Analysis. Thy1-YFPH transgenic mice (8–10 d old) were used to prepare organotypic hippocampal slices using the interface method. Dendritic spine density was evaluated as described previously (37, 40) (*SI Materials and Methods*).

Quantitative Confocal Immunohistochemistry. To determine the in situ integrity of the presynaptic and dendritic complex of the hippocampus and neocortex, 40-μm-thick vibratome sections were cut from paraformaldehyde-fixed brain and were immunolabeled with mouse monoclonal antibodies against synaptophysin (SY38; 1:500; Millipore) and MAP2 (1:100; Millipore) (*SI Materials and Methods*).

Western Blot Analysis of Tau, Phospho-Tau, and Caspase-3. sNMDARs and eNMDARs (by exposure to 100 μM NMDA) or oligomerized $A\beta_{1-42}$ (by exposure to 250 μM NMDA) were stimulated for 15 min to 1 h; then cell lysates were prepared as described previously (3). Western blots were probed for phospho-tau (AT8; Thermo), tau (TAU-5; Millipore), cleaved caspase-3 (Cell Signaling), and actin (Millipore) (*SI Materials and Methods*).

Neurobehavioral Analysis. The novel object exploration tests included the location novelty recognition test and the object novelty recognition tests to assess spatial learning as well as object learning (*SI Materials and Methods*).

HPLC Analysis of Glutamate Concentration. After 30 min incubation in oligomerized $A\beta_{1-42}$, culture medium was boiled and cleared by centrifugation (10,000 × *g* for 10 min) to remove insoluble materials. Subsequently, samples were diluted in 20 mM borate buffer at pH 9.0 and were derivatized for 1 min with *N*-tert-butyloxycarbonyl-L-cysteine and *o*-phthaldialdehyde. Samples then were separated in a 5-mm C18 reverse-phase column (220 × 4.6 mm) Sheri-5 (Brownlee), and glutamate was monitored by fluorescence (334 nm excitation and 433 nm emission) using an L-7485 detector (Hitachi).

Memantine and NitroMemantine Treatment. Mice were treated with memantine or NitroMemantine as previously described (*SI Materials and Methods*) (3).

In Vivo Microdialysis. All procedures were conducted in accordance with Institutional Animal Care and Use Committee (IACUC) guidelines. Microdialysis procedures were performed as previously described (67) on 12-mo-old and 20- to 24-mo-old male and female mice of the following genotypes: hAPP tg, α7KO, and hAPP tg/α7KO (23). Dialysate samples were analyzed as previously reported (68) (*SI Materials and Methods*).

Statistical Analysis. A Student *t* test was used for two-way comparisons, and an ANOVA with Tukey's HSD test was used for multiple comparisons. For cumulative probability curves, comparisons were made using the Kolmogorov–Smirnov test. Results are expressed as mean ± SEM.

ACKNOWLEDGMENTS. We thank Zhiguo Nie for help with early electrophysiology slice experiments, Jeff Zaremba for help with FRET imaging experiments, Anthony Nutter and Brian Lee for help with microdialysis experiments, and members of the S.A.L. laboratory for helpful assistance and discussions. This work was supported in part by National Institutes of Health Grants P01 AG010436 (to S.F.H.); P50 AG005131 (to J.C.P.-C.); P01 DA017259 and R01 AA020404 (to L.H.P.); R01 NS050636 (to J.W.K.); and P01 HD29587 and P01 ES016738 and Department of Defense Grant W81XWH-10-1-0093 (to S.A.L.). We also acknowledge the support of National Institute of Neurological Disorders and Stroke Institutional Core Grant P30 NS076411. P.X. and X.Z. were supported in part by American Heart Association fellowships, and S.S.-B was supported in part by a fellowship from the Ministry of Education and Science of Spain.

1. Li S, et al. (2011) Soluble Aβ oligomers inhibit long-term potentiation through a mechanism involving excessive activation of extrasynaptic NR2B-containing NMDA receptors. *J Neurosci* 31(18):6627–6638.
2. Palop JJ, Mucke L (2010) Amyloid-β-induced neuronal dysfunction in Alzheimer's disease: from synapses toward neural networks. *Nat Neurosci* 13(7):812–818.
3. Okamoto S, et al. (2009) Balance between synaptic versus extrasynaptic NMDA receptor activity influences inclusions and neurotoxicity of mutant huntingtin. *Nat Med* 15(12):1407–1413.
4. Milnerwood AJ, et al. (2010) Early increase in extrasynaptic NMDA receptor signaling and expression contributes to phenotype onset in Huntington's disease mice. *Neuron* 65(2):178–190.
5. Hardingham GE, Fukunaga Y, Bading H (2002) Extrasynaptic NMDARs oppose synaptic NMDARs by triggering CREB shut-off and cell death pathways. *Nat Neurosci* 5(5):405–414.
6. Hardingham GE, Bading H (2010) Synaptic versus extrasynaptic NMDA receptor signalling: implications for neurodegenerative disorders. *Nat Rev Neurosci* 11(10):682–696.
7. Tampellini D, et al. (2009) Synaptic activity reduces intraneuronal β, promotes APP transport to synapses, and protects against β-related synaptic alterations. *J Neurosci* 29(31):9704–9713.
8. Tampellini D, et al. (2010) Effects of synaptic modulation on β-amyloid, synaptophysin, and memory performance in Alzheimer's disease transgenic mice. *J Neurosci* 30(43):14299–14304.

9. Wroge CM, Hogins J, Eisenman L, Mennerick S (2012) Synaptic NMDA receptors mediate hypoxic excitotoxic death. *J Neurosci* 32(19):6732–6742.
10. Wei W, et al. (2010) Amyloid β from axons and dendrites reduces local spine number and plasticity. *Nat Neurosci* 13(2):190–196.
11. Jo J, et al. (2011) $A\beta_{1\text{-}42}$ inhibition of LTP is mediated by a signaling pathway involving caspase-3, Akt1 and GSK-3β. *Nat Neurosci* 14(5):545–547.
12. Tilleux S, Hermans E (2007) Neuroinflammation and regulation of glial glutamate uptake in neurological disorders. *J Neurosci Res* 85(10):2059–2070.
13. Matos M, Augusto E, Oliveira CR, Agostinho P (2008) Amyloid-β peptide decreases glutamate uptake in cultured astrocytes: involvement of oxidative stress and mitogen-activated protein kinase cascades. *Neuroscience* 156(4):898–910.
14. Song MS, Rauw G, Baker GB, Kar S (2008) Memantine protects rat cortical cultured neurons against β-amyloid-induced toxicity by attenuating tau phosphorylation. *Eur J Neurosci* 28(10):1989–2002.
15. Li S, et al. (2009) Soluble oligomers of amyloid β protein facilitate hippocampal long-term depression by disrupting neuronal glutamate uptake. *Neuron* 62(6):788–801.
16. Orellana JA, et al. (2011) ATP and glutamate released via astroglial connexin 43 hemichannels mediate neuronal death through activation of pannexin 1 hemichannels. *J Neurochem* 118(5):826–840.
17. Hires SA, Zhu Y, Tsien RY (2008) Optical measurement of synaptic glutamate spillover and reuptake by linker optimized glutamate-sensitive fluorescent reporters. *Proc Natl Acad Sci USA* 105(11):4411–4416.
18. Scheiffele P, Fan J, Choih J, Fetter R, Serafini T (2000) Neuroligin expressed in nonneuronal cells triggers presynaptic development in contacting axons. *Cell* 101(6): 657–669.
19. Patneau DK, Mayer ML (1990) Structure-activity relationships for amino acid transmitter candidates acting at N-methyl-D-aspartate and quisqualate receptors. *J Neurosci* 10(7):2385–2399.
20. Shankar GM, et al. (2008) Amyloid-β protein dimers isolated directly from Alzheimer's brains impair synaptic plasticity and memory. *Nat Med* 14(8):837–842.
21. Parpura V, et al. (1994) Glutamate-mediated astrocyte-neuron signalling. *Nature* 369 (6483):744–747.
22. Wang HY, et al. (2000) β-$Amyloid_{1\text{-}42}$ binds to α7 nicotinic acetylcholine receptor with high affinity. Implications for Alzheimer's disease pathology. *J Biol Chem* 275(8): 5626–5632.
23. Dziewczapolski G, Glogowski CM, Masliah E, Heinemann SF (2009) Deletion of the α 7 nicotinic acetylcholine receptor gene improves cognitive deficits and synaptic pathology in a mouse model of Alzheimer's disease. *J Neurosci* 29(27):8805–8815.
24. Sharma G, Vijayaraghavan S (2001) Nicotinic cholinergic signaling in hippocampal astrocytes involves calcium-induced calcium release from intracellular stores. *Proc Natl Acad Sci USA* 98(7):4148–4153.
25. Renner M, et al. (2010) Deleterious effects of amyloid β oligomers acting as an extracellular scaffold for mGluR5. *Neuron* 66(5):739–754.
26. Herman MA, Nahir B, Jahr CE (2011) Distribution of extracellular glutamate in the neuropil of hippocampus. *PLoS ONE* 6(11):e26501.
27. Papadia S, et al. (2008) Synaptic NMDA receptor activity boosts intrinsic antioxidant defenses. *Nat Neurosci* 11(4):476–487.
28. Xia P, Chen H-SV, Zhang D, Lipton SA (2010) Memantine preferentially blocks extrasynaptic over synaptic NMDA receptor currents in hippocampal autapses. *J Neurosci* 30(33):11246–11250.
29. Rosenmund C, Clements JD, Westbrook GL (1993) Nonuniform probability of glutamate release at a hippocampal synapse. *Science* 262(5134):754–757.
30. Maskell PD, Speder P, Newberry NR, Bermudez I (2003) Inhibition of human α 7 nicotinic acetylcholine receptors by open channel blockers of N-methyl-D-aspartate receptors. *Br J Pharmacol* 140(7):1313–1319.
31. Abramov E, et al. (2009) Amyloid-β as a positive endogenous regulator of release probability at hippocampal synapses. *Nat Neurosci* 12(12):1567–1576.
32. Hsieh H, et al. (2006) AMPAR removal underlies Aβ-induced synaptic depression and dendritic spine loss. *Neuron* 52(5):831–843.
33. Cissé M, et al. (2011) Reversing EphB2 depletion rescues cognitive functions in Alzheimer model. *Nature* 469(7328):47–52.
34. Wang Y, et al. (2006) The pharmacology of aminoadamantane nitrates. *Curr Alzheimer Res* 3(3):201–204.
35. Dawson VL, Dawson TM, London ED, Bredt DS, Snyder SH (1991) Nitric oxide mediates glutamate neurotoxicity in primary cortical cultures. *Proc Natl Acad Sci USA* 88(14): 6368–6371.
36. Lipton SA, et al. (1993) A redox-based mechanism for the neuroprotective and neurodestructive effects of nitric oxide and related nitroso-compounds. *Nature* 364 (6438):626–632.
37. Cho DH, et al. (2009) S-Nitrosylation of Drp1 mediates β-amyloid-related mitochondrial fission and neuronal injury. *Science* 324(5923):102–105.
38. Qu J, et al. (2011) S-Nitrosylation activates Cdk5 and contributes to synaptic spine loss induced by β-amyloid peptide. *Proc Natl Acad Sci USA* 108(34):14330–14335.
39. Choi YB, et al. (2000) Molecular basis of NMDA receptor-coupled ion channel modulation by S-nitrosylation. *Nat Neurosci* 3(1):15–21.
40. Shankar GM, et al. (2007) Natural oligomers of the Alzheimer amyloid-β protein induce reversible synapse loss by modulating an NMDA-type glutamate receptor-dependent signaling pathway. *J Neurosci* 27(11):2866–2875.
41. Lee HK, Kameyama K, Huganir RL, Bear MF (1998) NMDA induces long-term synaptic depression and dephosphorylation of the GluR1 subunit of AMPA receptors in hippocampus. *Neuron* 21(5):1151–1162.
42. Massey PV, et al. (2004) Differential roles of NR2A and NR2B-containing NMDA receptors in cortical long-term potentiation and long-term depression. *J Neurosci* 24 (36):7821–7828.
43. Kollen M, Dutar P, Jouvenceau A (2008) The magnitude of hippocampal long term depression depends on the synaptic location of activated NR2-containing N-methyl-D-aspartate receptors. *Neuroscience* 154(4):1308–1317.
44. Papouin T, et al. (2012) Synaptic and extrasynaptic NMDA receptors are gated by different endogenous coagonists. *Cell* 150(3):633–646.
45. Rosenberg D, et al. (2013) Neuronal D-serine and glycine release via the Asc-1 transporter regulates NMDA receptor-dependent synaptic activity. *J Neurosci* 33(8): 3533–3544.
46. Roberson ED, et al. (2007) Reducing endogenous tau ameliorates amyloid β-induced deficits in an Alzheimer's disease mouse model. *Science* 316(5825):750–754.
47. Tomiyama T, et al. (2010) A mouse model of amyloid β oligomers: their contribution to synaptic alteration, abnormal tau phosphorylation, glial activation, and neuronal loss in vivo. *J Neurosci* 30(14):4845–4856.
48. Ittner LM, et al. (2010) Dendritic function of tau mediates amyloid-β toxicity in Alzheimer's disease mouse models. *Cell* 142(3):387–397.
49. Zempel H, Thies E, Mandelkow E, Mandelkow EM (2010) Aβ oligomers cause localized Ca^{2+} elevation, missorting of endogenous Tau into dendrites, Tau phosphorylation, and destruction of microtubules and spines. *J Neurosci* 30(36):11938–11950.
50. Hoover BR, et al. (2010) Tau mislocalization to dendritic spines mediates synaptic dysfunction independently of neurodegeneration. *Neuron* 68(6):1067–1081.
51. Hyman BT (2011) Caspase activation without apoptosis: insight into Aβ initiation of neurodegeneration. *Nat Neurosci* 14(1):5–6.
52. Jin M, et al. (2011) Soluble amyloid β-protein dimers isolated from Alzheimer cortex directly induce Tau hyperphosphorylation and neuritic degeneration. *Proc Natl Acad Sci USA* 108(14):5819–5824.
53. Morris M, Maeda S, Vossel K, Mucke L (2011) The many faces of tau. *Neuron* 70(3): 410–426.
54. Roberson ED, et al. (2011) Amyloid-β/Fyn-induced synaptic, network, and cognitive impairments depend on tau levels in multiple mouse models of Alzheimer's disease. *J Neurosci* 31(2):700–711.
55. Sydow A, et al. (2011) Tau-induced defects in synaptic plasticity, learning, and memory are reversible in transgenic mice after switching off the toxic Tau mutant. *J Neurosci* 31(7):2511–2525.
56. D'Amelio M, et al. (2011) Caspase-3 triggers early synaptic dysfunction in a mouse model of Alzheimer's disease. *Nat Neurosci* 14(1):69–76.
57. Shleper M, Kartvelishvily E, Wolosker H (2005) D-Serine is the dominant endogenous coagonist for NMDA receptor neurotoxicity in organotypic hippocampal slices. *J Neurosci* 25(41):9413–9417.
58. LaFerla FM, Oddo S (2005) Alzheimer's disease: Aβ, tau and synaptic dysfunction. *Trends Mol Med* 11(4):170–176.
59. Bordji K, Becerril-Ortega J, Nicole O, Buisson A (2010) Activation of extrasynaptic, but not synaptic, NMDA receptors modifies amyloid precursor protein expression pattern and increases amyloid-ß production. *J Neurosci* 30(47):15927–15942.
60. Verges DK, Restivo JL, Goebel WD, Holtzman DM, Cirrito JR (2011) Opposing synaptic regulation of amyloid-β metabolism by NMDA receptors in vivo. *J Neurosci* 31(31): 11328–11337.
61. Lipton SA, Kater SB (1989) Neurotransmitter regulation of neuronal outgrowth, plasticity and survival. *Trends Neurosci* 12(7):265–270.
62. Kwon HB, Sabatini BL (2011) Glutamate induces de novo growth of functional spines in developing cortex. *Nature* 474(7349):100–104.
63. Kurup P, et al. (2010) Aβ-mediated NMDA receptor endocytosis in Alzheimer's disease involves ubiquitination of the tyrosine phosphatase STEP61. *J Neurosci* 30(17): 5948–5957.
64. Okita K, et al. (2011) A more efficient method to generate integration-free human iPS cells. *Nat Methods* 8(5):409–412.
65. Lin T, et al. (2009) A chemical platform for improved induction of human iPSCs. *Nat Methods* 6(11):805–808.
66. Usui K, et al. (2009) Site-specific modification of Alzheimer's peptides by cholesterol oxidation products enhances aggregation energetics and neurotoxicity. *Proc Natl Acad Sci USA* 106(44):18563–18568.
67. Abdallah L, et al. (2009) Impact of serotonin 2C receptor null mutation on physiology and behavior associated with nigrostriatal dopamine pathway function. *J Neurosci* 29 (25):8156–8165.
68. Song P, Mabrouk OS, Hershey ND, Kennedy RT (2012) In vivo neurochemical monitoring using benzoyl chloride derivatization and liquid chromatography-mass spectrometry. *Anal Chem* 84(1):412–419.

Supporting Information

Talantova et al. 10.1073/pnas.1306832110

SI Materials and Methods

Cell Cultures. Mixed neuronal/glial rat cerebrocortical cultures were prepared as previously described (1). To produce the glutamate-sensor probe, HEK 293T cells were grown in DMEM supplemented with 10% (vol/vol) fetal bovine serum (FBS), 1% penicillin and streptomycin, and were kept in a humidified 5% CO_2/95% air atmosphere incubator at 37 °C. Exponentially growing cells were trypsinized, seeded at 1×10^5 cells per well, and co-transfected with both SuperGluSnFR and neuroligin plasmids (1 μg each per well) using 1 μL Lipofectamine 2000 (Invitrogen). Primary cultures of purified rat or mouse astrocytes were prepared from 1- to 3-d-old animals and were cultured following standard protocols (2, 3). Primary human astrocytes were purchased from a commercial source and were cultured using reagents provided by the supplier (normal human astrocytes; Lonza). For glutamate FRET assays, we used cells 24–48 h post-transfection. Autaptic cultures were prepared following established methods (4–6). Primary hippocampal neurons were harvested from newborn rat pups at postnatal day 0 and were plated as a single-cell suspension on dot-shaped microislands made of primary rat astrocytes (7).

Generation of Human Induced Pluripotent Stem Cell-Derived Neurons from Dermal Fibroblasts. Differentiation into $NeuN^+$, $Tbr1^+$ cortical neurons was performed using a modified protocol (8). Briefly, feeder-free human induced pluripotent stem cells were treated with small-molecule inhibitors of bone morphogenetic protein (Dorsomorphin), Activin/Nodal (A83-01), and β-catenin (PNU-74654) for ∼1 wk. The $PAX6^+$ cells then were cultured for ∼3 wk as floating neurospheres in the presence of basic FGF (20 ng/mL), and subsequently adhered to form a monolayer on p-ornithine/laminin-coated dishes. They then were purified by FACS for $CD24^+/CD184^+/CD44^-/CD271^-/CD15_{low}$ cells and were seeded onto glass coverslips for terminal differentiation into mature neurons in the presence of medium supplemented with N2 and B27 (Invitrogen), BDNF (10 ng/mL), and glial cell line-derived neurotrophic factor (GDNF, 10 ng/mL). Neurons were cultured on a bed of astrocytes for the experiments described here.

Glutamate FRET Imaging. We used FRET microscopy with the SuperGluSnFR probe to monitor glutamate release from mixed neuronal/glial and pure astrocyte cultures using a modification of the astrocyte-HEK cell sensor assay (9). To detect release of glutamate from astrocytes, purified primary astrocytes were plated on top of HEK-293 cells expressing SuperGluSnFR plus the cell-adhesion protein neuroligin (10), the latter to increase cell–cell apposition. Under these conditions, we were able to detect changes in glutamate concentration within a wide dynamic range from 300 nM to 100 μM. Experiments were performed on an inverted microscope (Axiovert 100M; Zeiss) equipped for epifluorescence microscopy. Images were deconvolved using SlideBook software (Intelligent Imaging Innovations). Coverslips containing 14- to 21-d-old primary cultured cells were placed on the stage, and light was delivered to the sample through a 63× oil immersion objective (1.4 NA). Cells were superfused continuously at room temperature (22 °C) with standard medium containing (in mM) NaCl, 146; KCl, 2.5; NaOH, 4; $CaCl_2$, 1; D-glucose, 20; sucrose, 20; Hepes, 10; adjusted to pH 7.4. Drugs and reagents were added using a local microperfusion system (Warner Instruments). Cells were epi-illuminated alternately at 434 and 514 nm, and emitted light was collected at 527 nm for YFP and 476 nm for CFP. The peak CFP/YFP ratio was divided by the baseline CFP/YFP ratio and plotted after baseline normalization to 1. Images were obtained every second after a 400-ms stimulus. A 2×2 binning method was used to improve signal-to-noise ratio and minimize photobleaching.

Amyloid-β Peptide Preparations. Briefly, amyloid-β peptide (Aβ) was suspended to an initial concentration of 1 mM in hexafluoroisopropanol and incubated for 2 h at room temperature, and solvent was evaporated in a SpeedVac. Peptide was resuspended in dry DMSO to a final stock concentration of 5 mM and was kept frozen at −80 °C until use. For oligomerization, the stock solution was diluted 10-fold in MEM (GIBCO) and was then incubated at 4 °C for ≥24 h. Oligomerized Aβ peptide preparations were sonicated immediately before use. The total concentration of $Aβ_{1–42}$ was monitored by ELISA after centrifugation at $11{,}000 \times g$ for 2 min. Western blot and light-scattering analyses of the preparations were performed before and after centrifugation. For experiments, both monomeric and oligomeric synthetic $Aβ_{1–42}$ were diluted in physiological buffer. $Aβ_{25–35}$ and the control peptide $Aβ_{35–25}$ (Anaspec) were dissolved at a concentration of 10 mM in dry DMSO, diluted to a stock solution of 0.5 mM with purified water, and then further diluted in physiological buffer for experiments. For Western blot analysis, monomeric or oligomeric $Aβ_{1–42}$ peptides were subjected to electrophoresis using 10–20% (wt/vol) Novex Tricine gels (Invitrogen), and membranes were probed with monoclonal anti–β-amyloid (1:250, clone 6E10, Covance).

Measuring $Aβ_{1–42}$ Oligomer Concentration by Dynamic Light Scattering. In brief, 100 μL of either monomeric or oligomeric synthetic $Aβ_{1–42}$ (nominally 0.5 mM) was added to 4.9 mL of Dulbecco's PBS and was filtered through a 0.22-μm syringe-driven filter. Samples were placed in a Dawn EOS light-scattering photometer that led to a WyattQELS dynamic light-scattering instrument (Wyatt Technology). Dynamic light-scattering data were measured at an angle of 108° and were collected for each sample for at least 15 min. Data were assessed using the regularization analysis program QELS-Batch version 1.0.3 and are presented as fractional light-scattering intensity vs. hydrodynamic radius.

Electrophysiology. Horizontal hippocampal slices were prepared from 13- to 14-wk-old WT and hAPP-J20 transgenic mice. Brains were removed under isoflurane anesthesia and were placed in ice-cold buffer equilibrated with 95% O_2 and 5% CO_2 consisting of (in mM) sucrose, 246; KCl, 2; NaH_2PO_4, 1.25; $NaHCO_3$, 26; D-glucose, 10; $MgSO_4$, 2; $CaCl_2$, 0.5; Na-L-ascorbate, 1; pH 7.4. We then cut 350-μm-thick slices with a vibratome (VT1000S; Leica), and slices recovered at room temperature for at least 1 h before recording in equilibrated (95% O_2 and 5% CO_2) artificial cerebrospinal fluid (aCSF) recording solution consisting of (in mM) NaCl, 124, KCl, 3; NaH_2PO_4, 1.25; $NaHCO_3$, 26; D-glucose, 10; $MgCl_2$, 0.5–1; $CaCl_2$, 2; pH 7.4. Recordings were obtained at room temperature from neurons lying superficial in the slice within 1–6 h of preparation. To monitor miniature excitatory postsynaptic currents (mEPSCs), slices were superfused at 2 mL/min with nominally magnesium-free, equilibrated aCSF supplemented with 50 μM picrotoxin and 1 μM TTX for at least 20 min before recording. CA1 neurons were visualized under differential interference contrast optics. Whole-cell patch-clamp recordings were performed using 3- to 5-MΩ pipettes filled with an internal solution composed of (in mM) K-gluconate, 120; KCl, 15; $MgCl_2$, 1; Hepes, 5; EGTA; 5; Mg-ATP, 2; pH 7.4, mOsm

290. To record glutamatergic tonic basal currents in hippocampal slices, CA1 neurons were held at −70 mV in nominally magnesium-free aCSF. After obtaining a stable recording, either 100 μM 3-[(R)-2-carboxypiperazin-4-yl]-propyl-1-phosphonic acid (CPP)/50 μM 6-cyano-7-nitroquinoxaline-2,3-dione (CNQX), 50 μM (D-)-2-amino-5-phosphonovalerate (D-APV)/10 μM 2,3-dihydroxy-6-nitro-7-sulfamoyl-benzo[f]quinoxaline (NBQX), or 10 μM memantine was perfused into the slices by bath application. Because of its better tissue penetration, the NMDA receptor (NMDAR) antagonist CPP generally was used rather than APV. The mean glutamatergic basal current amplitude was measured by the addition of these specific antagonists.

To record field excitatory postsynaptic potentials (fEPSPs), a tungsten bipolar electrode was used to stimulate the Schaffer collateral-commissural pathway with constant current pulses of 0.05-ms duration to evoke fEPSPs. fEPSPs were recorded at room temperature by placing a patch pipette in the stratum radiatum of the CA1 region at least 60–80 μm away from the cell body layer. Input/output (I/O) curves were generated by plotting the 10–90% slope of fEPSP vs. stimulation intensity. To study paired pulse facilitation (PPF), two stimuli were applied at an interval of 50 ms. The paired pulse ratio (PPR) was determined by the quotient of the mean amplitude of the second fEPSP to the first. All controls were run on the same day as experimental drugs.

Neurons were superfused constantly at a rate of 2 mL/min with a Hepes-buffered external solution composed of (in mM): NaCl, 146; KCl, 2.5; $CaCl_2$, 2; D-glucose, 20; Hepes, 10; adjusted to pH 7.4 with NaOH, 300–310 mOsm. Patch pipettes were pulled from borosilicate glass capillaries (G150F-3; Warner Instruments) using a micropipette puller (P87; Sutter Instruments) and had open tip resistances of 2–7 MΩ with an internal solution composed of (in mM) CsCl, 140; NaCl, 4; $CaCl_2$, 0.5; EGTA, 5; Hepes, 10; Na-GTP, 0.5; Mg-ATP, 2; adjusted to pH 7.33 with CsOH; 315 mOsm. In some experiments, we used a Cs-gluconate–based intracellular solution composed of (in mM) Cs-gluconate, 117; NaCl, 9; Hepes, 10; EGTA, 10; and $MgCl_2$, 2; adjusted to pH 7.2 with NaOH. NMDAR-mediated currents were recorded in the nominal absence of extracellular magnesium and in the presence of 10–20 μM glycine.

To quantify mEPSCs in autaptic neurons, the preparation was superfused with 1 μM TTX for at least 20 min to allow for equilibration before recording.

Intracellular NO and Intracellular Ca^{2+} Measurements. Primary cultured rat cortical cells (14–21 d in culture) were loaded for 2 h at room temperature with Fura-2/AM (4 μM) or for 30 min with diaminofluorescein (DAF) FM diacetate (2.5 μM; Molecular Probes) in imaging buffer containing (in mM): NaCl, 146; KCl, 2.5; NaOH, 4; CaCl2, 1; D-glucose, 20; sucrose, 20; Hepes, 10; adjusted to pH 7.4. After loading, the cells were washed twice with imaging buffer. For Fura-2–based measurements of intracellular calcium changes, we used a liquid light guide connected to an ultra high-speed wavelength switcher fitted with a 175 Watt xenon arc lamp (Lambda DG4; Sutter Instrument) and an optimized Fura-2 filter set for obtaining the 350/380 nm excitation ratio. For NO measurements, DAF-loaded cells were excited using a standard GFP filter set (470 nm peak/40 nm bandwidth), and emissions were collected above 510 nm. For analysis, images were collected using a CCD camera mounted on a Zeiss Axiovert 35 microscope and analyzed with SlideBook software. Fluorescence values were calculated as changes in fluorescence ratios relative to baseline fluorescence intensity ($\Delta F/F_0$). For each experiment, values were calculated by dividing the change in peak fluorescence (ΔF) over resting baseline fluorescence (F_0); in other words, fluorescence values represented fractional changes above baseline ($\Delta F/F_0$). These values were plotted as arbitrary units (a.u.).

Dendritic Spine Analysis. Brains were dissected out under isoflurane anesthesia, and 350-μm-thick hippocampal slices were collected in ice-cold dissection buffer containing (in mM): sucrose, 212; KCl, 3; $MgCl_2$, 5; $CaCl_2$, 0.5; NaH_2PO_4, 1; $NaHCO_3$, 26; D-glucose, 10. Dissection buffer was bubbled with 95% O_2/5% CO_2. Slices were transferred onto a Millicell cell-culture insert (Millipore) and were placed in medium 1 containing Eagle's Minimum Essential Medium [50% (vol/vol)], horse serum [25% (vol/vol)], Earle's Balanced Salt Solution [18% (vol/vol)], D-glucose (32–35 mM), Hepes (25 mM), glutamine (2 mM), Amphotericin B (2.5 μg/mL), and streptomycin sulfate (100 μg/mL). After 24 h, the culture medium was changed to medium 2 of similar composition but containing a lower concentration of horse serum [5% (vol/vol)]. Thereafter, every 2–3 d, half of the culture medium was replaced with fresh medium 2. Slices were exposed to oligomerized $A\beta_{1-42}$ peptide containing 500-nM oligomers, memantine (10 μM), or NitroMemantine (10 μM) for 7 d, replenished accordingly with each medium replacement. Similarly, glycine or D-serine–degrading enzymes were replenished when used instead of NMDAR antagonists. Dendritic spine density was evaluated as follow: Slices were fixed in 4% paraformaldehyde, and images of YFP-expressing cells were acquired by deconvolution microscopy using SlideBook software. For YFP-expressing neurons (n >12 for each condition), two distinct fields of secondary or tertiary dendrites at least 40 μm in length were selected randomly and analyzed in a masked fashion using SlideBook analysis software.

Quantitative Confocal Immunohistochemistry. Primary antibodies were detected with the horse anti-mouse FITC antibody (1:75; Vector Laboratories) and mounted under glass coverslips using anti-fading medium (Vector Laboratories). Quantitative confocal immunofluorescence was used for analysis. All sections were processed under the same standardized conditions. Immunolabeled blind-coded sections were imaged serially using a laser-scanning confocal microscope and were analyzed with National Institutes of Health ImageJ 1.43 software. Three sections from each mouse were analyzed, and for each section, four fields in the frontal cortex and hippocampus were examined. For synaptophysin and MAP2, results are expressed as the percent area of the neuropil occupied by immunoreactive terminals and dendrites.

Western Blot Analysis of Tau, Phospho-Tau, and Caspase-3. Primary neurons were lysed in buffer [50 mM Tris (pH 7.5), 100 mM NaCl, 1% Nonidet P-40, 10% (vol/vol) glycerol, 1 mM EDTA, 4 mM sodium orthovanadate, 20 mM β-glycerophosphate disodium salt hydrate, 100 nM calyculin A, 2 mM Pefabloc SC, Thermo Fisher Phosphatase inhibitor mixture, and Sigma Protease inhibitor mixture]. The lysates were spun down at 15,000 × g for 20 min, and the supernatant was collected. Protein concentration was determined by bicinchoninic acid protein assay (Thermo). Equal amounts of protein for each sample were run on NuPAGE Novex 4–12% (wt/vol) Bis-Tris Gel (Invitrogen) and were transferred to nitrocellulose membranes (GE Healthcare). All membranes were blocked in SuperBlock (Thermo). Blots were probed for phospho-tau (AT8; Thermo), tau (TAU-5; Millipore), cleaved caspase-3 (Cell Signaling), and actin (Millipore). The protein signal from the membranes was measured using SuperSignal West Dura (Thermo) and was quantified digitally. In these experiments, synaptic NMDARs (sNMDARs) were stimulated via inhibition of inhibitory transmission with bicuculline (see above). After isolation of extrasynaptic NMDARs (eNMDARs) (as described above), these receptors were stimulated by exposure to NMDA (100 μM) or oligomerized $A\beta_{1-42}$ (250 nM) for 15–60 min, and then cell lysates were prepared.

Neurobehavioral Analysis. We performed the location novelty recognition test (NL) (11, 12) to assess the ability of mice to recognize a novel spatial arrangement of familiar objects; this test is sensitive to hippocampal damage (13, 14). Mice were individually habituated to a 51 × 51 × 39 cm open field for 5 min. For the familiarization trials, three plastic toy objects were placed in the open field (one in each of three corners), and an individual animal was allowed to explore for 5 min. After three familiarization trials (separated by 1 min in a holding cage), the mouse was tested in a location novelty recognition test in which one of the familiar objects was moved to a novel location in the arena. The same object was moved to the same new location for every mouse tested. All objects and the arena were thoroughly cleaned with 70% (vol/vol) ethanol between trials to remove odors. The three different objects required for this study were chosen based on previously published methods (11); there was no statistically significant preference for any object in pilot studies using C57BL/6J mice. The number of contacts made with each object was defined as nose-first approaches within 2–4 cm of the object. Habituation to the objects across the three familiarization trials (decreased contacts) is an initial measure of learning, and the renewed interest (increased contacts) in the moved object is evidence of spatial memory.

Memantine and NitroMemantine Treatment. Mice were injected i.p. twice daily at 12-h intervals with PBS (vehicle control) or a solution of either memantine or NitroMemantine in PBS, both equimolar at 216 mmol/kg body weight (a dose equivalent to 1 mg/kg twice a day of memantine, which was calculated to produce an effective concentration at synapses of ≤10 μM) (15). Solutions were prepared fresh daily, and a total volume of 10 μL/g body weight was injected. Injections started at 6 mo of age and continued for 3 mo, followed by behavioral testing, electrophysiological recording, and histological analysis.

In Vivo Microdialysis. A microdialysis probe was stereotaxically implanted into the right hippocampus, under isoflurane anesthesia, using the following coordinates (in millimeters from bregma) (16): AP = −2.0, ML = −1.3, DV = −2.0. Dialysis probes were perfused continuously using a syringe pump (PHD 22/2000; Harvard Apparatus) with aCSF composed of (in mM): NaCl, 149; KCl, 2.8; $CaCl_2$, 1.2; $MgCl_2$, 1.2; glucose, 5.4; ascorbic acid, 0.25; pH 7.2–7.4. An 18-h postimplantation period of recovery was allowed before dialysate collection; during this period, aCSF was perfused at a constant rate of 0.15 μL/min. The next day the perfusion speed was increased to 0.6 μL/min, and a 2-h presampling period was allowed before dialysate was sampled for analysis. Six baseline dialysate samples were collected in polypropylene tubes at 10-min intervals over a 60-min period (17, 18). Dialysate samples were placed in dry ice immediately and were stored at −80 °C until glutamate content was analyzed using liquid chromatography coupled with tandem mass spectrometry (LC-MS/MS) as previously reported, with minor modifications. Briefly, dialysate samples (2 μL) were supplanted with 5.5 μL of 100 mM borate and then were reacted with 2% (vol/vol) benzoyl chloride (2.5 μL), quenched with 2% (vol/vol) formic acid (2.5 μL), and supplemented with $^{13}C_6$-benzoyl chloride–labeled internal standard (2.5 μL). Derivatized samples (12 μL) were separated by HPLC (Agilent 1260) on a Zorbax rapid-resolution high-definition (RRHD) column (2.1-mm internal diameter × 50 mm in length, 1.8-μm particle size; 50 °C) using 10 mM ammonium formate (0.15% formic acid) for mobile phase A and acetonitrile for mobile phase B as follows: 0% B (0 min), 0% B (3 min), 65% B (7 min), 65% B (8.50 min), 0% B (8.51 min), 0% B (13.25 min). Eluents were analyzed for the constituents of interest using MS/MS (Agilent 6460 with JetStream ion source). Quantification was performed by isotope dilution using the following standard curve: 250, 500, 1,000, 2,000 nM.

1. Cho DH, et al. (2009) S-Nitrosylation of Drp1 mediates β-amyloid-related mitochondrial fission and neuronal injury. *Science* 324(5923):102–105.
2. McAllister AK (2000) Biolistic transfection of neurons. *Sci STKE* 2000(51):pl1.
3. McCarthy KD, de Vellis J (1980) Preparation of separate astroglial and oligodendroglial cell cultures from rat cerebral tissue. *J Cell Biol* 85(3):890–902.
4. Segal MM, Furshpan EJ (1990) Epileptiform activity in microcultures containing small numbers of hippocampal neurons. *J Neurophysiol* 64(5):1390–1399.
5. Segal MM (1991) Epileptiform activity in microcultures containing one excitatory hippocampal neuron. *J Neurophysiol* 65(4):761–770.
6. Bekkers JM, Stevens CF (1991) Excitatory and inhibitory autaptic currents in isolated hippocampal neurons maintained in cell culture. *Proc Natl Acad Sci USA* 88(17):7834–7838.
7. Xia P, Chen H-SV, Zhang D, Lipton SA (2010) Memantine preferentially blocks extrasynaptic over synaptic NMDA receptor currents in hippocampal autapses. *J Neurosci* 30(33):11246–11250.
8. Chambers SM, et al. (2009) Highly efficient neural conversion of human ES and iPS cells by dual inhibition of SMAD signaling. *Nat Biotechnol* 27(3):275–280.
9. Pasti L, Zonta M, Pozzan T, Vicini S, Carmignoto G (2001) Cytosolic calcium oscillations in astrocytes may regulate exocytotic release of glutamate. *J Neurosci* 21(2):477–484.
10. Scheiffele P, Fan J, Choih J, Fetter R, Serafini T (2000) Neuroligin expressed in nonneuronal cells triggers presynaptic development in contacting axons. *Cell* 101(6):657–669.
11. Benice TS, Rizk A, Kohama S, Pfankuch T, Raber J (2006) Sex-differences in age-related cognitive decline in C57BL/6J mice associated with increased brain microtubule-associated protein 2 and synaptophysin immunoreactivity. *Neuroscience* 137(2):413–423.
12. Benice TS, Raber J (2008) Object recognition analysis in mice using nose-point digital video tracking. *J Neurosci Methods* 168(2):422–430.
13. Save E, Poucet B, Foreman N, Buhot MC (1992) Object exploration and reactions to spatial and nonspatial changes in hooded rats following damage to parietal cortex or hippocampal formation. *Behav Neurosci* 106(3):447–456.
14. Save E, Buhot MC, Foreman N, Thinus-Blanc C (1992) Exploratory activity and response to a spatial change in rats with hippocampal or posterior parietal cortical lesions. *Behav Brain Res* 47(2):113–127.
15. Okamoto S-i, et al. (2009) Balance between synaptic versus extrasynaptic NMDA receptor activity influences inclusions and neurotoxicity of mutant huntingtin. *Nat Med* 15(12):1407–1413.
16. Paxinos G, Franklin KBJ (2001) *The Mouse Brain in Stereotaxic Coordinates* (Academic, San Diego), 2nd Ed.
17. Rocha BA, et al. (2002) Enhanced locomotor, reinforcing, and neurochemical effects of cocaine in serotonin 5-hydroxytryptamine 2C receptor mutant mice. *J Neurosci* 22(22):10039–10045.
18. Ramchandani VA, et al. (2011) A genetic determinant of the striatal dopamine response to alcohol in men. *Mol Psychiatry* 16(8):809–817.

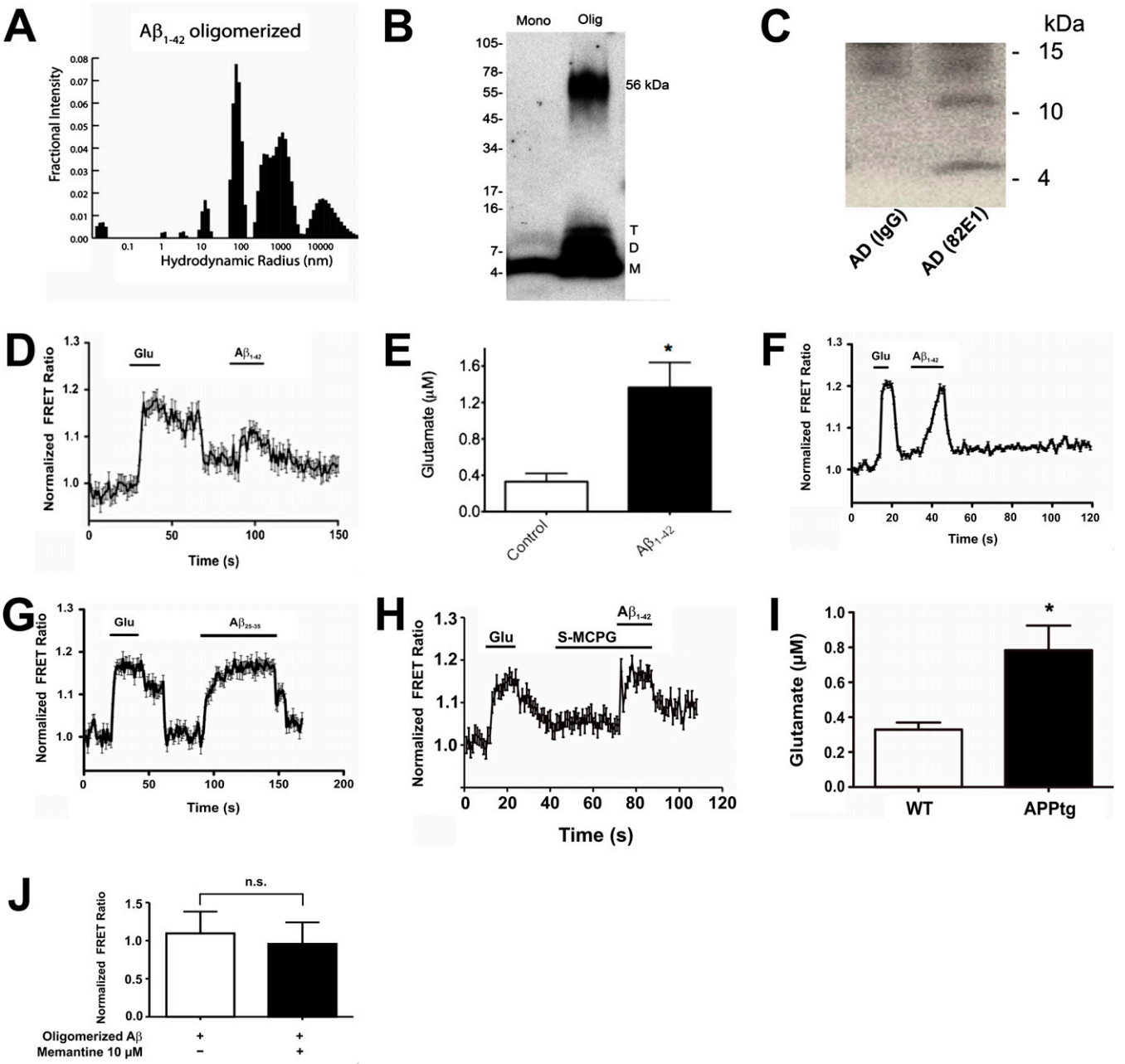

Fig. S1. Aβ preparations and effect on astrocyte glutamate release. (*A*) Regularization analysis representing the size distribution of particles in synthetic $A\beta_{1–42}$ preparations, as measured by dynamic light scattering. Peaks represent different-sized particles after $A\beta_{1–42}$ was oligomerized (*Materials and Methods*). The peaks at 1.35 ± 0.15 nm and 4.49 ± 0.66 nm likely represent residual monomers, and these peaks together comprise 1.1% of the total light-scattering intensity. The peak at 18.2 ± 3.7 nm, likely representing small oligomers of $A\beta_{1–42}$, comprises ∼5% of the total light-scattering intensity and ∼15% of the soluble fraction (which was the fraction used in the physiological experiments in the present study). The peak located at just under 100 nm likely represents soluble amyloid fibrils. The soluble fraction obtained after centrifugation no longer contained peaks at >100 nm, which likely represent large amyloid fibrils. (*B*) Immunoblot characterization of monomeric and oligomeric synthetic $A\beta_{1–42}$ peptides under denaturing (SDS) conditions. Monomeric (*Left*; Mono) or oligomeric (*Right*; Olig) $A\beta_{1–42}$ peptides (∼88 ng each) were electrophoresed and immunoblotted using clone 6E10 monoclonal antibody against Aβ. The monomeric Aβ preparation revealed only one predominant immunoreactive band corresponding to the size of Aβ monomer. The oligomeric Aβ preparation displayed multiple immunoreactive bands corresponding to the size of Aβ monomers (M), dimers (D), trimers (T), and dodecamers (56 kDa). Relative molecular masses (kDa) are shown at left. (*C*) Naturally occurring oligomeric Aβ detected in brain extracts by immunoblot analysis of postmortem human brains with late-onset Alzheimer's disease. (*Left*) Control IgG antibody pull down. (*Right*) Aβ 82E1 monoclonal antibody pull down. By this analysis, primarily dimers and trimers of $A\beta_{1–42}$ were observed. (*D*) Glutamate release induced by low concentrations of synthetic $A\beta_{1–42}$ oligomers. Normalized ratio of FRET intensity, representing glutamate release from purified rat astrocytes, induced by 325 pM oligomeric $A\beta_{1–42}$ (in a solution containing 6 nM total $A\beta_{1-42}$). Glutamate standard (Glu) represents the nearly saturated FRET response to ≥30 μM glutamate. Data are shown as mean ± SEM; $n = 32$ cells analyzed in five experiments. (*E*) HPLC measurements of glutamate released from mouse astrocyte cultures incubated with Aβ oligomers. Astrocytes were incubated with 250 nM oligomeric $A\beta_{1–42}$ for 30 min. Medium then was collected and filtered, and HPLC measurements performed. $n = 9$ samples analyzed; $^*P < 0.05$. (*F*) Aβ-induced glutamate release from astrocytes is not dependent on microglia/macrophages. Synthetic oligomeric Aβ (250 nM) in the presence of L-leucine methyl ester (7.5 mM for 24 h) to deplete monocytoid cells still induced release of glutamate in purified rat astrocyte cultures, as monitored by measurement of the normalized FRET ratio. Glutamate standard (Glu) represents the nearly saturated FRET response to ≥30 μM glutamate. Values are mean ± SEM; $n = 24$ cells analyzed in three experiments. (*G*) $A\beta_{25–35}$ (10 μM) peptide induces glutamate release from

Legend continued on following page

purified rat astrocytes by measurement of the normalized FRET ratio. Glutamate standard (Glu) represents the nearly saturated FRET response to ≥30 μM glutamate. Data are shown as mean ± SEM; $n = 61$ cells analyzed in six experiments. (*H*) Oligomeric $A\beta_{1–42}$ (500 nM) induced glutamate release from purified astrocytes in the presence of the metabotropic glutamate receptor antagonist (S)-α-methyl-4-carboxyphenylglycine (S-MCPG; 500 μM). Data are shown as mean ± SEM; $n = 15$ cells analyzed in three experiments. (*I*) In vivo microdialysis showed that basal levels of extracellular glutamate were higher in the hippocampus of ∼12-mo-old transgenic mice overexpressing human APP (hAPP tg) than in age-matched WT mice (mean + SEM; $n = 4$; $^*P < 0.05$). (*J*) Memantine (10 μM) manifests a minor effect on glutamate release from astrocytes induced by 250 nM oligomeric $A\beta_{1–42}$, as monitored by the FRET probe. The figure shows the area under the curve for FRET ratios for mouse astrocytes exposed to oligomerized $A\beta_{1–42}$ alone ($n = 19$ cells) or to $A\beta_{1–42}$ in the presence of 10 μM memantine ($n = 12$ cells). Values represent mean + SEM from three different experiments for each condition. FRET ratios were normalized to 1 and plotted as a function of time for the duration of the response. Although there was a trend for memantine to decrease glutamate release in the face of $A\beta_{1–42}$ exposure, it did not reach statistical significance. n.s., not significant.

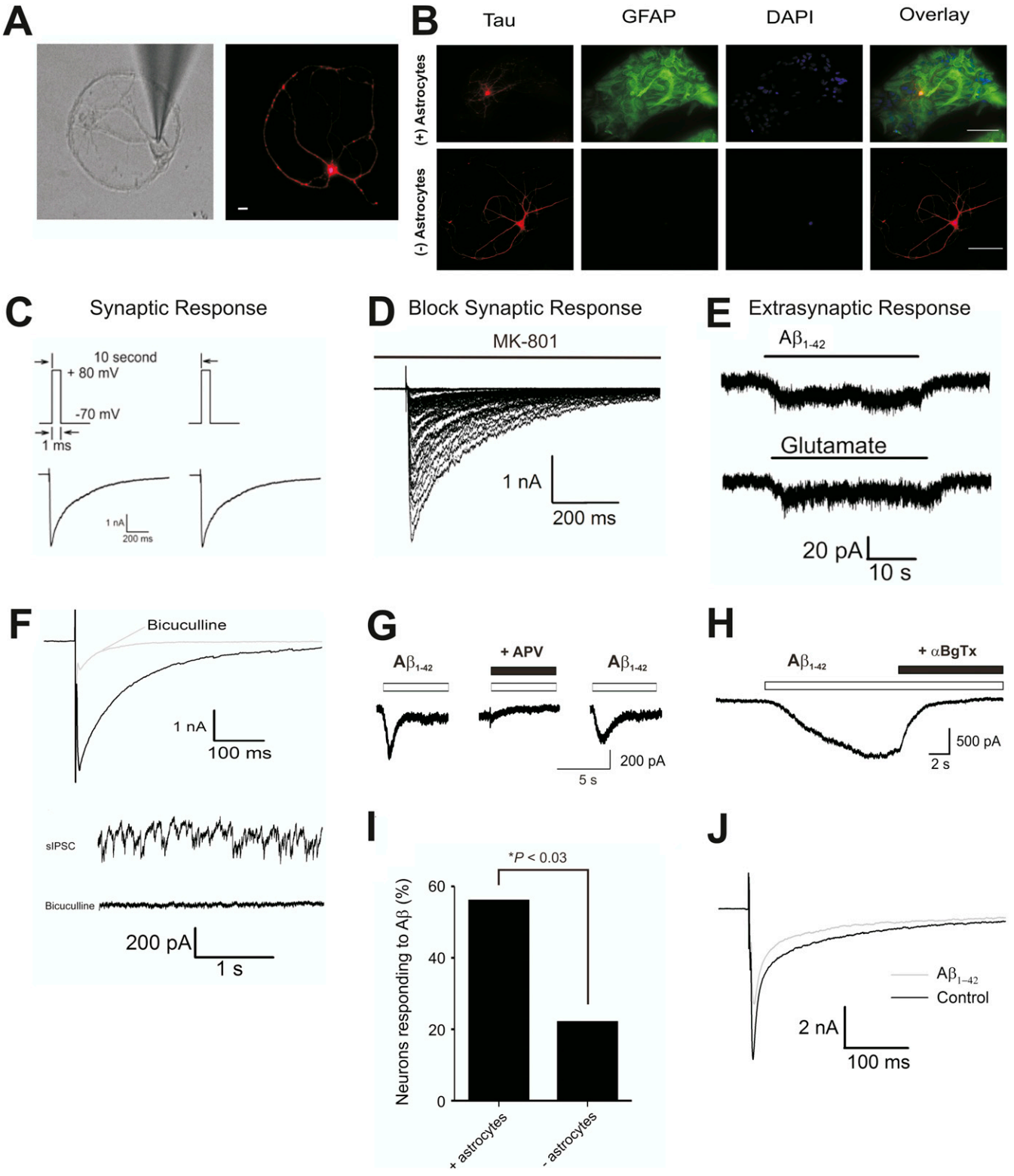

Fig. S2. Effect of Aβ on synaptic and extrasynaptic receptor activity in autaptic hippocampal cultures. (*A*) Representative hippocampal autaptic cultures. (*Left*) Phase-contrast photomicrograph during recording with a patch electrode. (*Right*) Immunofluorescence with Tau antibody. (Scale bar: 20 μm.) (*B*) Representative hippocampal autaptic cultures with and without astrocytes (immunofluorescence with Tau and GFAP antibodies, nuclei labeled with DAPI). (Scale bar: 100 μm.) Note that the neurites on the bed of astrocytes are difficult to visualize in the upper panel because they are out of the focal plane. (*C*) During recording with a patch electrode, synaptic NMDA R-mediated responses in autaptic cultures were induced using a stimulation protocol consisting of 1-ms depolarizations from −70 mV to +80 mV in the presence of 10 μM NBQX in the absence of extracellular Mg^{2+}. (*D*) Synaptic NMDARs then were blocked by 10 μM dizocilpine (MK-801) applied during repeated synaptic stimulation, whereas extrasynaptic NMDARs were spared. (*E*) Subsequent applications of oligomerized $A\beta_{1-42}$ or glutamate then were shown to induce extrasynaptic currents. (*F*) Characterization of inhibitory GABAergic autaptic hippocampal neurons. In this case, unlike the excitatory autaptic neurons, bicuculline (20 μM) antagonized the evoked inhibitory postsynaptic current (IPSC), indicating the GABAergic

Legend continued on following page

nature of this neuron (*top traces*). Spontaneous miniature IPSCs (*middle trace*) also were blocked by bicuculline (*bottom trace*). (*G* and *H*) Application of synthetic $A\beta_{1–42}$ (containing 250-nM oligomers) induced inward currents in neurons derived from human induced pluripotent stem cells (hiPSCs) voltage-clamped at −70 mV and plated on a bed of astrocytes; these currents were blocked by 50 μM D-APV or by 100 nM α-bungarotoxin (α-BgTx). (*I*) Histogram comparison of autaptic neurons responding to oligomerized Aβ when plated in the presence or absence of astrocytes. Approximately 56% of neurons on astrocytes produced a detectable extrasynaptic current in response to oligomerized Aβ compared with 22% of neurons not on astrocytes. A Fisher's exact text for a 2×2 contingency table summarizing the results indicated that neurons plated on astrocytes were significantly more likely to respond to oligomerized Aβ than neurons not on astrocytes. $n = 109$ neurons tested; one-tailed $P < 0.03$. Note that the currents also were much larger for neurons plated on astrocytes than for neurons not on astrocytes (not shown). (*J*) Synthetic $A\beta_{1–42}$ (containing 500-nM oligomers) induced a decrease in the amplitude of evoked excitatory postsynaptic current (EPSC) in hippocampal autaptic neurons within tens of seconds. Both the early AMPA receptor (AMPAR)-mediated and late NMDAR-mediated components of the EPSC were affected.

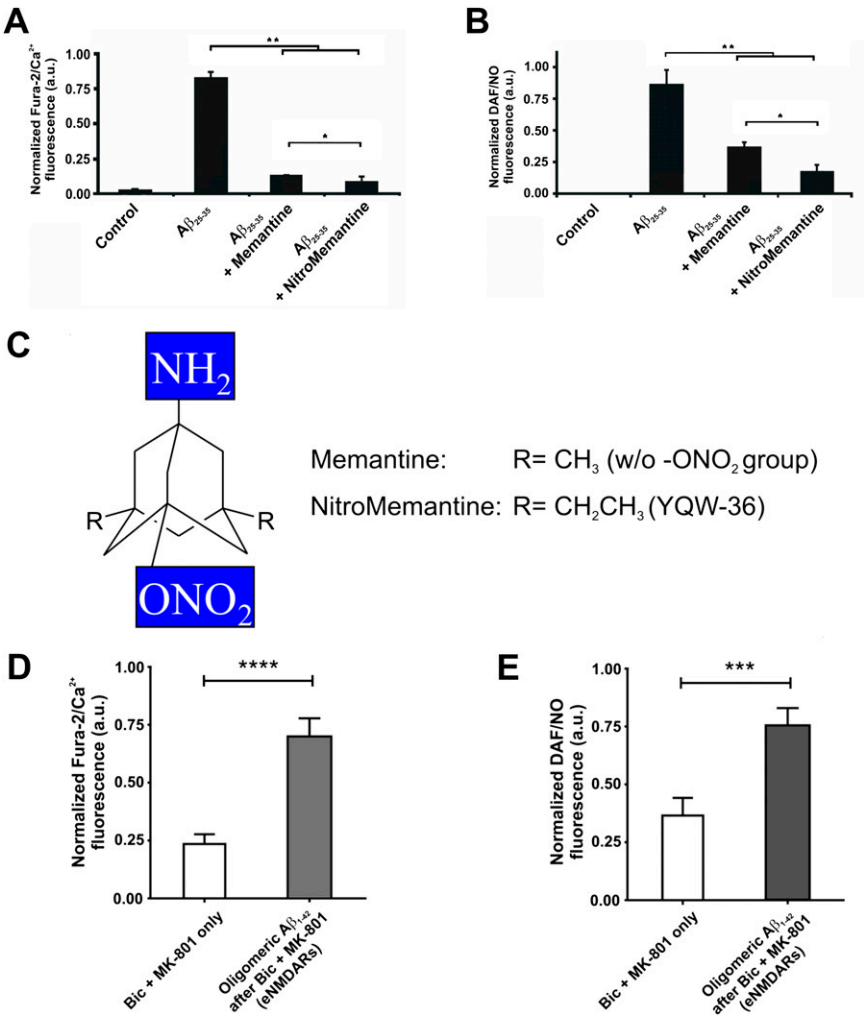

Fig. S3. Aβ activation of eNMDARs increases intracellular Ca^{2+} and NO in primary neurons. (*A* and *B*) Change in Fura-2 and DAF fluorescence intensity with the addition of $A\beta_{25–35}$ (10 μM) in the presence or absence of memantine or NitroMemantine (10 μM). Values are mean + SEM for all panels. $*P < 0.05$, $**P < 0.01$; $n = 11–40$ neurons for each condition. a.u., arbitrary units. (*C*) Structures of memantine and NitroMemantine (YQW-036) used in the current study. Note that the bridgehead amine group ($–NH_2$) in both drugs is protonated under physiological conditions to form NH_3^+ and is thought to interact at or near the Mg^{2+} binding site in the NMDAR-associated channel. The R (methyl) groups in memantine were lengthened to ethyl groups in NitroMemantine, because this change was found to compensate for a loss in channel affinity engendered by the addition of the $–ONO_2$ nitro group. The $–ONO_2$ group provides increased efficacy for NitroMemantine via a second site of action at the redox-modulatory sites of the NMDAR in addition to its primary site of action as an open-channel blocker via the memantine moiety (1–8). (*D* and *E*) eNMDAR-mediated increases in Ca^{2+} and NO in rat primary cerebrocortical neurons induced by synthetic $A\beta_{1–42}$ oligomers. To isolate eNMDARs, sNMDARs were activated via disinhibition with a brief application of bicuculline (50 μM) followed by blockade with the long-lasting NMDAR inhibitor MK-801 (10 μM). After bicuculline and MK-801 were washed out, oligomeric $A\beta_{1–42}$ (250 nM) was added while intracellular Ca^{2+} and intracellular NO were monitored by Fura-2 and DAF fluorescence, respectively. Values are mean + SEM. $***P < 0.001$, $****P < 0.0001$; $n \geq 19$ neurons for each condition. a.u., arbitrary units.

1. Chen H-SV, Lipton SA (1997) Mechanism of memantine block of NMDA-activated channels in rat retinal ganglion cells: Uncompetitive antagonism. *J Physiol* 499(Pt 1):27–46.
2. Chen H-SV, Lipton SA (2005) Pharmacological implications of two distinct mechanisms of interaction of memantine with N-methyl-D-aspartate-gated channels. *J Pharmacol Exp Ther* 314(3):961–971.
3. Chen H-SV, Lipton SA (2006) The chemical biology of clinically tolerated NMDA receptor antagonists. *J Neurochem* 97(6):1611–1626.
4. Choi Y-B, et al. (2000) Molecular basis of NMDA receptor-coupled ion channel modulation by S-nitrosylation. *Nat Neurosci* 3(1):15–21.
5. Choi Y-B, Chen HV, Lipton SA (2001) Three pairs of cysteine residues mediate both redox and Zn^{2+} modulation of the NMDA receptor. *J Neurosci* 21(2):392–400.
6. Takahashi H, et al. (2007) Hypoxia enhances S-nitrosylation-mediated NMDA receptor inhibition via a thiol oxygen sensor motif. *Neuron* 53(1):53–64.
7. Wang Y, et al. (2006) The pharmacology of aminoadamantane nitrates. *Curr Alzheimer Res* 3(3):201–204.
8. Lipton SA (2006) Paradigm shift in neuroprotection by NMDA receptor blockade: Memantine and beyond. *Nat Rev Drug Discov* 5(2):160–170.

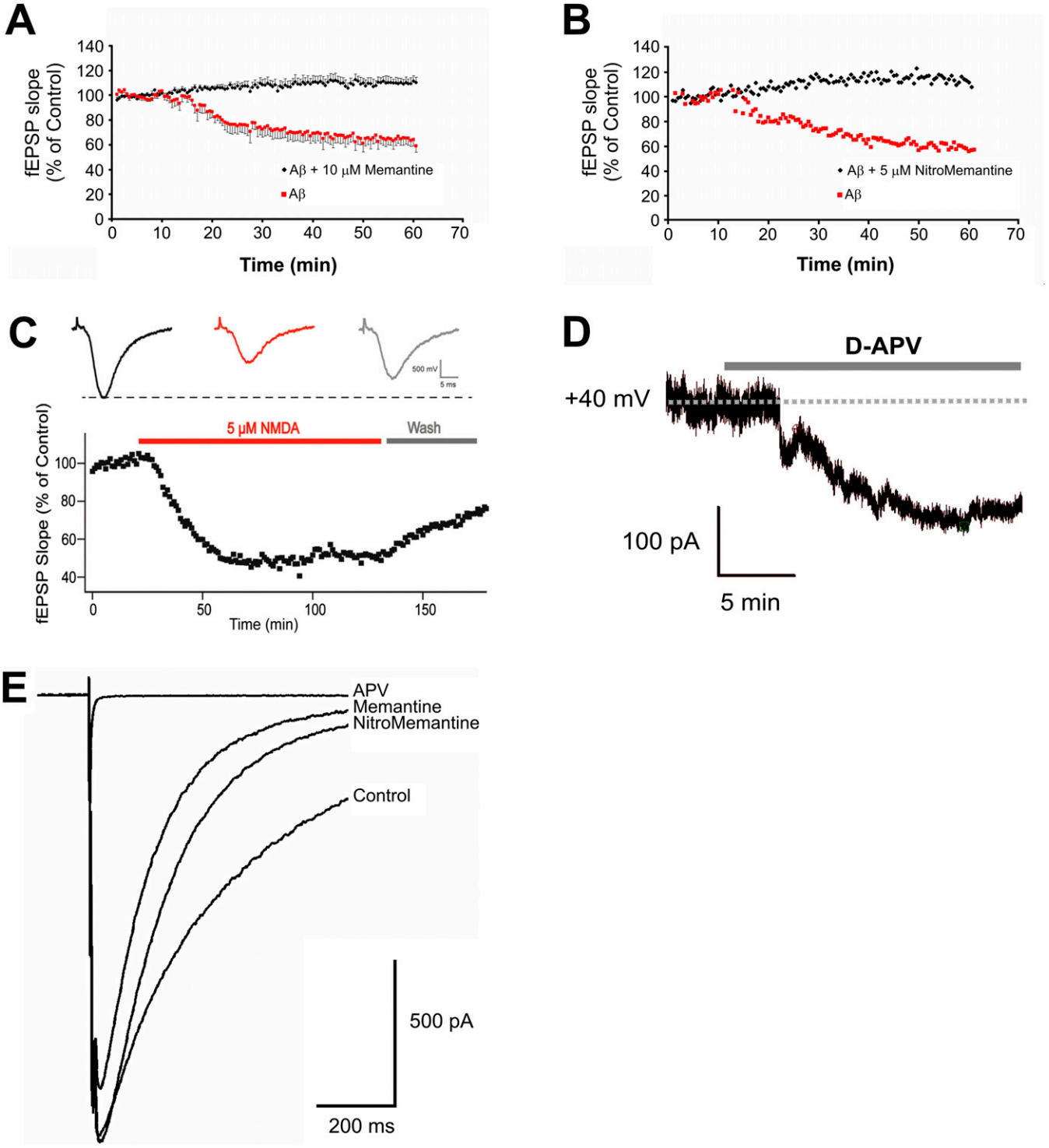

Fig. S4. Memantine and NitroMemantine antagonize the effects of Aβ on synaptic transmission. (*A*) Memantine (10 μM) antagonized Aβ-induced synaptic depression in hippocampal slices. Time course of fEPSP slope showing the effect of 500 nM $A\beta_{25-35}$ added 10 min after the beginning of the recording. Values are mean + SEM. (*B*) NitroMemantine (5 μM) antagonized the effect of Aβ on synaptic depression in the hippocampus. Time course of the fEPSP slope after the addition of 500 nM $A\beta_{25-35}$ beginning 10 min into the recording. (*C*) Synaptic depression induced by application of exogenous NMDA to hippocampal slice. The upper panel shows representative traces, and the lower panel shows the time course of the fEPSP slope before and after the addition of 5 μM NMDA. fEPSPs were evoked every 30 s by stimulating the Schaffer collateral-commissural pathway with constant current pulses and were recorded in the stratum radiatum of the CA1 region at least 60–80 μm away from the cell body layer. (*D*) Application of 50 μM D-APV blocks the basal current in hAPP-J20 tg mouse hippocampal slices. Notice the decrease in the noise level (rms level: 4.9 pA before D-APV, and 2.4 pA after D-APV), reflecting blockade of NMDAR-associated channels. Holding potential, +40 mV in the presence of 10 μM NBQX to isolate the NMDAR-mediated component of the current. (*E*) NitroMemantine (10 μM) blocks less sNMDAR-mediated current than memantine (10 μM) in the hippocampal autapse preparation. The NMDAR-mediated component of evoked EPSCs was isolated by recording in the presence of 10 μM NBQX to block AMPAR-mediated currents. The competitive NMDAR antagonist D-APV (50 μM) virtually completely blocked sNMDARs, but memantine manifested substantially less effect. NitroMemantine blocked even less of the sNMDAR-mediated current than equimolar memantine under these conditions.

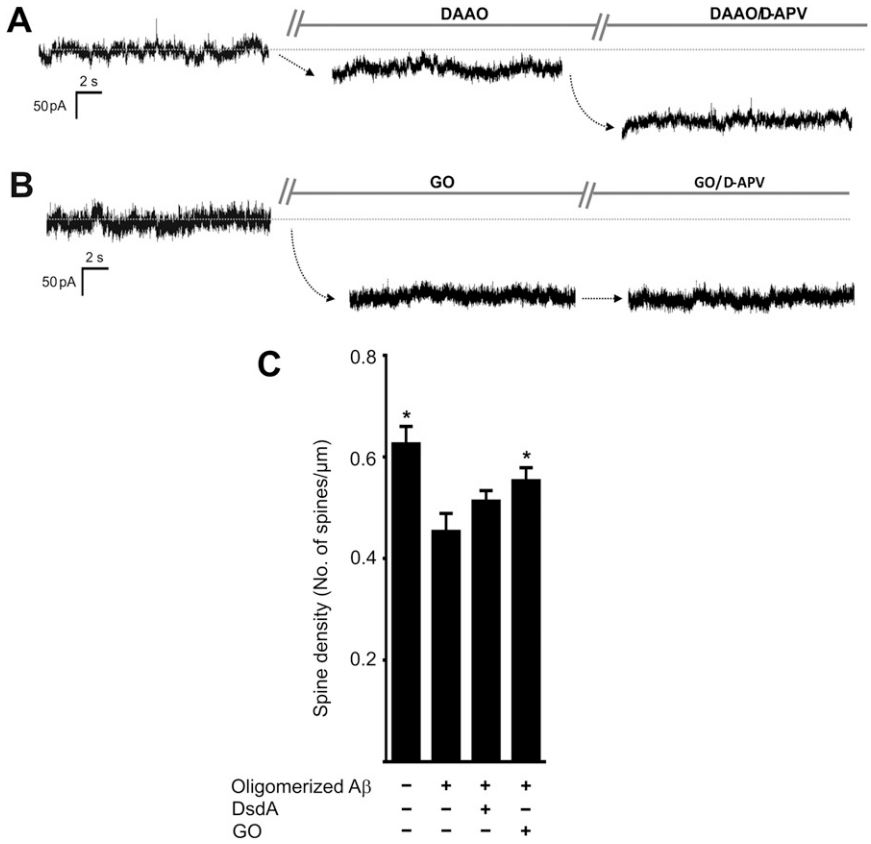

Fig. S5. Effect of the degradation of D-serine versus glycine on NMDAR-mediated basal current and dendritic spine loss in hAPP-J20 tg hippocampal slices. (*A*) Incubation of slices with 1 unit/mL D-amino acid oxidase (DAAO) did not substantially affect the basal current, but the addition of 50 μM D-APV blocked the basal current. (*B*) Incubation in 41 μg/mL glycine oxidase (GO) for ∼1 h resulted in significant block of the basal current. Addition of 50 μM D-APV did not significantly increase the degree of block. In both *A* and *B*, the protocol to isolate the NMDAR-mediated component of the current (voltage-clamp at +40 mV in the presence of 1 mM Mg^{2+}, 10 μM NBQX, 50 μM picrotoxin, and 1 μM TTX) and the amounts of enzyme used were similar to those previously reported (1). Line breaks indicate the incubation time in the enzyme (≥20 min) required to see an effect on hippocampal brain slices. (*C*) Enzymatic degradation of the eNMDAR coagonist glycine significantly reduced the loss of dendritic spines produced by oligomerized Aβ in hippocampal slices, but degradation of the sNMDAR coagonist D-serine did not. Hippocampal slices from YFP-tg mice were exposed for 7 d to control or synthetic $A\beta_{1-42}$ (500-nM oligomers) in the presence or absence of enzymes that hydrolyze D-serine (D-serine deaminase, DsdA, 30 μg/mL) or glycine (glycine oxidase, GO, 41 μg/mL); $n = 55$, $^*P < 0.05$ by *t* test with Bonferroni correction.

1. Papouin T, et al. (2012) Synaptic and extrasynaptic NMDA receptors are gated by different endogenous coagonists. *Cell* 150(3):633–646.